# Calciprotein particle-induced calcium overload triggers mitochondrial dysfunction in endothelial cells

Lian Feenstra, Laurent Chatre, Benoit Bernay, Julien Pontin, Mirjam F Mastik, Azuwerus van Buiten, Dalibor Nakládal, Bastiaan S Star, Jan-luuk Hillebrands, Guido Krenning

The Journal of Physiology



# Calciprotein particle-induced calcium overload triggers mitochondrial dysfunction in endothelial cells

Lian Feenstra[1], Laurent Chatre[2], Benoit Bernay[3], Julien Pontin[3], Mirjam F. Mastik[1], Azuwerus van Buiten[4], Dalibor Nakládal[5], Bastiaan S. Star[4], Jan-Luuk Hillebrands[1] and Guido Krenning[4]

[1]*Department of Pathology and Medical Biology, University of Groningen, University Medical Center Groningen, Groningen, the Netherlands*
[2]*Université de Caen Normandie, CNRS, Normandie Université, ISTCT, UMR 6030, GIP Cyceron, Caen, France*
[3]*Normandi Univ, UNICAEN, US EMerode, Plateforme Proteogen, Caen, France*
[4]*Department of Clinical Pharmacy and Pharmacology, University of Groningen, University Medical Center Groningen, Groningen, the Netherlands*
[5]*Clinical Research Unit, Comenius University Science Park, Bratislava, Slovakia*

Handling Editors: Kim Barrett & Luis Sobrevia

The peer review history is available in the Supporting Information section of this article (https://doi.org/10.1113/JP287656#support-information-section).

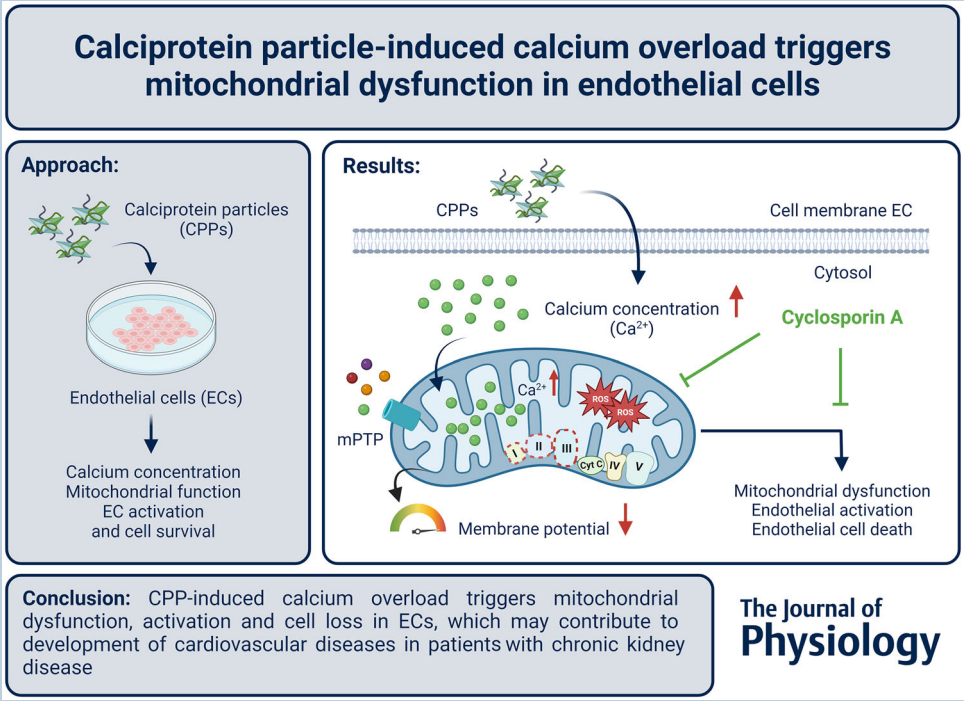


**Abstract figure legend** Calciprotein particles (CPPs) are small calcium- and phosphate-containing nanoaggregates associated with the development of vascular disease (CVD) in chronic kidney disease (CKD). Previously, we have shown that CPPs induce endothelial cell (EC) dysfunction, possibly contributing to CVD in CKD, but the underlying molecular mechanisms remain unknown. In the current study, we demonstrate that exposure of ECs to CPPs resulted in an increase of both cytosolic and mitochondrial calcium ($Ca^{2+}$) and altered mitochondrial processes including reduced mitochondrial respiration, mitochondrial membrane potential and antioxidant capacity. By using a mitochondrial permeability transition pore (mPTP) inhibitor, cyclosporin A, EC activation and cell death caused by CPPs could be attenuated. These data indicate that CPP-induced $Ca^{2+}$ overload is a key process in mitochondrial dysfunction, activation and cell death of ECs, which may contribute to CVD in CKD. Interventions targeting CPP-induced mitochondrial dysfunction might preserve EC function and alleviate vascular dysfunction in CKD.

 DOI: 10.1113/JP287656

**Abstract** Calciprotein particles (CPPs) are calcium- and phosphate-containing nanoparticles numbers of which are increased in patients with chronic kidney disease (CKD). CPPs have been associated with the development of vascular disease, although the underlying mechanisms are unknown. We previously showed that CPPs induce endothelial cell (EC) dysfunction by reducing nitric oxide (NO) bioavailability and generating superoxide ($O_2^{\cdot -}$). Here, we tested the hypothesis that CPPs induce mitochondrial calcium ($Ca^{2+}$) overload, which may trigger mitochondrial dysfunction and, consequently, EC activation. Exposure of human umbilical vein ECs to CPPs resulted in significantly increased cytosolic and mitochondrial $Ca^{2+}$ levels compared to vehicle-treated ECs. Proteome analysis demonstrated impaired endoplasmic reticulum calcium signalling, and decreased enrichment of proteins in the mitochondrial OXPHOS complexes I–III in CPP-exposed ECs. Respirometry data confirmed these findings and demonstrated decreased basal and maximal respiration in CPP-exposed ECs. This was accompanied by reduced mitochondrial membrane potential, reduced antioxidant capacity and loss of mitochondria. In the presence of cyclosporin A, a potent mitochondrial permeability transition pore inhibitor, CPP-induced EC activation and cell death were attenuated. Taken together, our data indicate that CPP-induced $Ca^{2+}$ overload is an important trigger of mitochondrial dysfunction, and EC activation and cell loss, which eventually may contribute to the development of vascular diseases in CKD. Interventions that target CPP-induced mitochondrial dysfunction might preserve EC function and possibly alleviate the development of vascular diseases in CKD.

(Received 8 September 2024; accepted after revision 7 February 2025; first published online 8 March 2025)
**Corresponding author** G. Krenning: Department of Clinical Pharmacy and Pharmacology, University of Groningen, University Medical Center Groningen, Hanzeplein 1 – AP50, 9713 GZ, Groningen, the Netherlands. Email: g.krenning@umcg.nl

## Key points

- Calciprotein particles (CPPs) are calcium- and phosphate-containing nanoparticles numbers of which are increased in patients with chronic kidney disease and which have been associated with the development of vascular disease.
- In this study, we tested the hypothesis that CPPs induce mitochondrial calcium ($Ca^{2+}$) overload in endothelial cells, thereby triggering mitochondrial dysfunction and endothelial activation.
- We show that exposure of HUVECs (human umbilical vein endothelial cells) to CPPs results in increased cytosolic and mitochondrial $Ca^{2+}$ levels, which is associated with alterations in mitochondrial processes (proteome analysis), cellular respiration, mitochondrial integrity and number.
- CPP-induced EC activation and cell death were attenuated in the presence of cyclosporin A, a potent mitochondrial permeability transition pore inhibitor.
- Our data indicate that CPP-induced $Ca^{2+}$ overload triggers mitochondrial dysfunction, endothelial activation and cell loss. Interventions that target CPP-induced mitochondrial dysfunction might preserve EC function in chronic kidney disease.

**Lian Feenstra** has been studying calciprotein particles (CPPs) since she was an undergraduate student. Determined to elucidate the role of endothelial cells in CPP-induced vascular calcification, she wrote her own PhD research proposal, which received funding from the University Medical Center Groningen in the Netherlands. Lian obtained her PhD degree in 2024 and is committed to continue contributing to novel insights in the field of CPPs.

## Introduction

Calciprotein particles (CPPs) are circulating calcium, phosphate and protein nanoparticles formed as a consequence of high phosphate levels in chronic kidney disease (CKD) (Holt & Smith, 2016; Kutikhin et al., 2021; Nakamura et al., 2022). Increasing levels of phosphate ($PO_4^{3-}$) can bind the circulating calcium ($Ca^{2+}$) and serum proteins (including Fetuin-A) and lead to the formation of amorphous calcium and phosphate complexes, which are initially defined as primary CPPs. Primary CPPs mature over time into the more noxious (crystalline) secondary CPPs (Holt & Smith, 2016; Kutikhin et al., 2021; Marreiros et al., 2022; Nakamura et al., 2022). Secondary CPPs are considered harmful for the cardiovascular system and have been associated with the development of vascular disease, including vascular calcification (VC) in CKD (Bundy, Cai, Mehta, et al., 2019; Keyzer et al., 2016; Smith et al., 2012, 2014). Previous research showed that increased serum calcification propensity (i.e. reduced $T_{50}$ score reflecting accelerated maturation from primary to secondary CPPs) in CKD patients was significantly associated with progressive aortic stiffening and all-cause mortality (Smith et al., 2014). Similarly, in a large cohort study of mild to severe CKD patients, higher calcification propensity was associated with the severity and progression of coronary artery calcification (Bundy, Cai, Scialla, et al., 2019). Although associations between secondary CPPs (hereafter CPPs) and calcification propensity have been clearly established over recent years, the molecular mechanisms and pathways on how CPPs contribute to the process of VC in CKD remain largely elusive.

Covering the lumen of the vasculature, endothelial cells (ECs) are exposed to circulating elements in the blood, including CPPs. *In vitro* studies show that exposure of ECs to CPPs leads to expression of EC-activation markers, intercellular adhesion molecule 1 (ICAM-1) and vascular cell adhesion molecule 1 (VCAM-1), and a change towards a pro-inflammatory phenotype, including secretion of pro-inflammatory cytokines IL-6 and IL-8 (Kutikhin et al., 2016; Shishkova et al., 2021; Thiem et al., 2023). Along with these observations, CPPs hamper the function of nitric oxide synthase 3 (eNOS) and decrease the bioavailability of nitric oxide (NO), features reminiscent of EC dysfunction (Feenstra et al., 2023). CPPs can be taken up by ECs from the environment (Kutikhin et al., 2016; Shishkova et al., 2021), ending up in lysosomes. Given the acidic pH in lysosomes, it is likely that the crystalline calcium phosphate nanoparticles disintegrate in the EC lysosomes (Shishkova et al., 2021). Additionally, endothelial activation and dysfunction are considered the instigators of the development of cardiovascular diseases (Medina-Leyte et al., 2021; Sun et al., 2020). As the uptake of CPPs by ECs has been associated with apoptosis (Kutikhin et al., 2016; Shishkova et al., 2021), but also with EC activation (Shishkova et al., 2021; Thiem et al., 2023) and dysfunction (Feenstra et al., 2023), CPP-induced effects on ECs might aggravate the development of cardiovascular disease including calcification in high-risk patients. The precise mechanisms linking endothelial CPP uptake to resulting activation and dysfunction are unclear, and potential targets for intervention have yet to be identified. Based on our own observations (Feenstra et al., 2023) and recent data published by others (Shishkova et al., 2023), we propose that mitochondria play a critical role in this process.

In ECs, the endoplasmic reticulum (ER) and mitochondria tightly interact to maintain intracellular $Ca^{2+}$ homeostasis (Giorgi et al., 2018; Tran et al., 2000). Cytosolic $Ca^{2+}$ can be taken up by the ER via the $Ca^{2+}$ ATPase pumps (SERCA) and released via opening of the inositol trisphosphate receptors ($IP_3Rs$) or ryanodine receptors (RyRs) (Giorgi et al., 2018; Tran et al., 2000). Release of $Ca^{2+}$ from the ER leads to high local concentrations of cytosolic $Ca^{2+}$, triggering nearby mitochondria to take up $Ca^{2+}$ from the environment, via voltage-dependent anion-selective channel proteins (VDACs) located on the outer mitochondrial membrane (MOM) (Feno et al., 2019; Giorgi et al., 2018). $Ca^{2+}$ subsequently enters the mitochondrial matrix via mitochondrial calcium uniporters (MCUs), located on the inner mitochondrial membrane (MIM), where the $Ca^{2+}$ is then stored in the mitochondrial matrix (Feno et al., 2019; Giorgi et al., 2018). Mitochondria are responsible for ∼25% of the intracellular $Ca^{2+}$ storage, and function as important regulators in modulating intracellular $Ca^{2+}$ homeostasis (Tran et al., 2000). However, in various pathological conditions, cytosolic $Ca^{2+}$ concentrations can rapidly rise, leading to mitochondrial $Ca^{2+}$ overload and subsequent mitochondrial dysfunction (Matuz-Mares et al., 2022; Murphy & Liu, 2023; Santulli et al., 2015). $Ca^{2+}$-induced mitochondrial dysfunction is characterized by an increased mitochondrial permeability, mitochondrial membrane depolarization, mitochondrial volume expansion (or swelling) and increased reactive oxygen species generation (ROS), which eventually leads to apoptosis (Feno et al., 2019). Whether CPPs induce mitochondrial $Ca^{2+}$ overload in ECs, leading to EC dysfunction, and whether this can be reduced or prevented by therapeutic targeting of mitochondria, is currently unknown.

In the present study, we hypothesized that CPPs increase the cytosolic $Ca^{2+}$ concentration of ECs, causing a mitochondrial $Ca^{2+}$ overload, impairment of mitochondrial function, and EC activation and loss. Identifying the underlying mechanism of CPP-induced endothelial activation and dysfunction is crucial to understand the fundamental pathways by which CPPs might

induce EC dysfunction, and conceivably contribute to the pathophysiology of VC in CKD in a paracrine manner.

## Methods

### Calciprotein particle generation

CPPs were generated as described previously (Feenstra et al., 2023). In brief, Dulbecco's modified eagle medium (DMEM) was enriched with 3.5 mM phosphate and 1 mM calcium, 10% fetal bovine extract (FBS), 1% penicillin-streptomycin, 1% sodium pyruvate and 1% non-essential amino acids (all v/v) and incubated for 14 days at 37°C with 5% $CO_2$. After 14 days, CPPs were isolated via centrifugation at 24 000 *g* at 4°C twice for 2 h. CPP concentration (μg calcium/mL) was based on the calcium content of the resuspended precipitate measured with the Calcium Colorimetric Assay kit (#MAK022, Sigma-Aldrich, St Louis, MO, USA). CPPs were characterized as detailed and reported by us earlier (Feenstra et al., 2023).

### Cell culture

Human umbilical vein endothelial cells (HUVECs, hereafter ECs) were purchased from Lonza (#CC-2519, Lonza, Basel, Switzerland) and cultured in endothelial cell culture medium (ECM) containing RPMI-1640 medium supplemented with 20% FBS (v/v), 1% penicillin-streptomycin (v/v), 1% L-glutamine (v/v), 5 U/mL heparin and 50 μg/mL homemade endothelial cell growth factor extract (ECGF) (Burgess et al., 1985). Cells were expanded in T75 culture flasks coated with 1% (w/v) gelatin solution at 37°C and 5% $CO_2$ (v/v). For *in vitro* experiments, ECs were seeded in T75 flasks, in multi-well plates or on (glass) coverslips. All experiments were performed under reduced serum conditions (i.e. ECM containing 5% (v/v) FBS) in the presence of 50 μg/mL CPPs or (1×) TBS (volume) control for 24 h.

### Cytosolic and mitochondrial calcium analysis

To visualize cytosolic and mitochondrial calcium ($Ca^{2+}$), cells were cultured on coverslips. After CPP exposure, particles were removed and cells were incubated with Fluo-4 AM (cytosolic $Ca^{2+}$, 2 μM, #ab241082, Abcam, Cambridge, UK) or Rhod-2 AM (mitochondrial $Ca^{2+}$, 4 μM, #ab142780, Abcam) for 60 min at 37°C, in the dark. Cells were washed with PBS, and subsequently fixed in 2% (w/v) paraformaldehyde (PFA). Coverslips were placed on StarFrost Microscope slides and mounted with Aqua-Poly/Mount mounting medium. Probes were visualized with a confocal laser scanning microscope (TCS SP8, Leica, Wetzlar, Germany) using a 63× objective.

To quantify alterations in cytosolic and mitochondrial $Ca^{2+}$ levels, cells were incubated with Fluo-4 AM (4 μM) or Rhod-2 AM (8 μM) for 60 min at 37°C in the dark, after CPP exposure. The excess probe was washed away with serum-free ECM and the fluorescent signal was measured at 494/506 nm (Fluo-4 AM) and 552/581 (Rhod-2 AM) excitation/emission using the FlexStation 3 multi-mode microplate reader (Molecular Devices, San Jose, CA, USA). Data were normalized to the experimental control.

### Cellular proteome analysis

To measure cellular proteome alterations after CPP exposure, proteins were extracted from ECs using RIPA buffer (#89900, ThermoFisher Scientific, Waltham, MA, USA) supplemented with a protease and phosphatase inhibitor cocktail (respectively #P8849 Sigma-Aldrich, #78420, ThermoFisher Scientific). Samples were vortexed for 30 s and sonicated for 3 × 5 s and the supernatant was collected after 10 min of centrifugation at 14,000 *g* and 4°C. Protein concentrations were measured with the protein colorimetric assay (#5000122, Bio-Rad, Hercules, CA, USA). Five micrograms of protein was prepared using the modified Gel-aided Sample Preparation, according to the previous protocol (Fischer & Kessler, 2015). Samples were digested with trypsin/Lys-C (25:1 protein:protease ratio, #V5071, Promega, Charbonnières-les-Bains, France) overnight at 37°C. For nano-LC fragmentation, protein or peptide samples were first desalted and concentrated onto a μC18 Omix (Agilent Technologies, Santa Clara, CA, USA) before analysis. Chromatography was performed on a NanoElute (Bruker Daltonics, Billirica, MA, USA) ultra-high-pressure nanoflow chromatography system. Approximatively 200 ng of each peptide sample was concentrated onto a C18 pepmap 100 (5 mm × 300 μm i.d.) precolumn (ThermoFisher Scientific) and separated at 50°C onto a reversed-phase Reprosil column (25 cm × 75 μm i.d.) packed with 1.6 μm C18 coated porous silica beads (IonOpticks, Collingwood, VIC, Australia). Mobile phases consisted of 0.1% formic acid, 99.9% (v/v) water (A) and 0.1% formic acid in 99.9% (v/v) acetonitrile (B). The nanoflow rate was set at 250 nL/min, and the gradient profile was as follows: from 2% to 30% B within 70 min, followed by an increase to 37% B within 5 min and further to 85% within 5 min and re-equilibration. MS experiments were carried out on a TIMS-TOF pro mass spectrometer (Bruker Daltonics) with a modified nano electrospray ion source (CaptiveSpray, Bruker Daltonics). A 1400 spray voltage with a capillary temperature of 180°C was typically employed for ionizing. MS spectra were acquired in the positive mode in the mass range from 100 to 1700 *m/z* and 0.60 to 1.60 1/*k*0 window. The mass spectrometer was operated in PASEF DIA mode with the exclusion of single

charged peptides. The DIA acquisition scheme consisted of 16 variable windows ranging from 400 to 1200 *m/z*.

## Protein identification and enrichment analysis

Database searching and Label Free Quantification (LFQ) (using extracted ion chromotography (XIC)) were performed using DIA-NN (version 1.6.0). An updated version of the UniProt *Homo sapiens* database was used for library-free search/library generation. For RT prediction and extraction mass accuracy, the default parameter 0.0, which means DIA-NN performed automatic mass and RT correction, was used. The top six fragments (ranked by their library intensities) were used for peptide identification and quantification. The false discovery rate (FDR) was set to 1% at the peptide precursor level. The variable modifications allowed were as follows: Nterm-acetylation and Carbamylation. In addition, C-Propionoamide was set as a fix modification. 'Trypsin/P' was selected. Data were filtered according to an FDR of 1%. Cross-run normalization was performed with RT-dependent. To quantify the relative levels of protein abundance between different groups, data from DIA-NN were then analysed using the DEP package in R. Briefly, proteins that are identified in three out of four replicates of at least one condition were filtered, data were normalized using a variance stabilizing transformation, missing data were imputed using random draws from a manually defined left-shifted Gaussian distribution, and differential enrichment analysis was based on linear models and empirical Bayes statistic. A fold increase $>1.5$ or $<-1.5$ in relative abundance and adjusted *P*-value $<0.05$ were used to determine enriched proteins.

Overall pathway enrichment for biological processes, molecular function and cellular compartment was performed for differentially abundant proteins using the full proteome as background in g:Profiler (g:GOst, version e111_eg58_p18_f463989d, Estonia) (Kolberg et al., 2023). Enrichments were considered statistically relevant at a FDR-adjusted *P*-value of $<0.05$.

Targeted enrichment analysis (GSEA) software version 4.1.0 (Broad Institute, Cambridge, MA, USA) (Mootha et al., 2003; Subramanian et al., 2005) was used for the MitoCarta3.0 dataset (Broad Institute) (mitochondrial protein enrichment), and curated datasets for calcium homeostasis [i.e. the EMBL-EBI annotated gene ontology set intracellular calcium ion homeostasis (i.e. GO:0006874) and the related gene ontology family sets on calcium-mediated signalling (GO:0019722), Golgi calcium ion homeostasis (GO:0032468), ER calcium ion homeostasis (GO:0032469), response to vitamin D (GO:0033280), vitamin D metabolic process (GO:0042359), regulation of cytosolic calcium ion concentration (GO:0051480) and mitochondrial calcium ion homeostasis (GO:00515560)]. The complete identified proteome was used for enrichment analysis. Enrichments were considered statistically relevant at an FDR-adjusted *P*-value of $<0.05$ and when the pathway included at least one differentially expressed protein (CPPs *vs*. unstimulated ECs).

## Immunoblotting OXPHOS complexes

Protein extraction for immunoblotting was performed in RIPA buffer (#89900, ThermoFisher Scientific) supplemented with a protease and phosphatase inhibitor cocktail (respectively #P8849 Sigma-Aldrich, #78420, ThermoFisher Scientific). Protein content was determined with the Bicinchoninic acid (BCA) Protein Assay kit (#23227, ThermoFisher Scientific/Pierce). In total, 10 µg protein was loaded for SDS/PAGE. After blotting, the Trans-blot Turbo nitrocellulose membrane (#1704270, Bio-Rad) was stained with Ponceau S staining solution for loading reference. Subsequently, the membrane was then blocked with blocking buffer [5% milk in 1× TBS (w/v), 0.1% Tween (v/v)] for 1 h. OXPHOS complexes were detected with the Total OXPHOS WB Antibody Cocktail primary antibodies (1:1000, #ab110413, Abcam) in blocking buffer overnight at 4°C. The HRP-conjugated secondary antibody (1:2000, #ab6789, Abcam) was used to detect the primary antibodies. Blot visualization was performed on an Odyssey Fc Imager (Li-Cor Biosciences, Lincoln, NE, USA). The signal was corrected for total protein input (Ponceau S) and normalized to the experimental control.

## High-resolution respirometry

High-resolution respirometry was performed to measure changes in mitochondrial respiratory function of ECs after CPP exposure. Cells were detached from T75 culture flasks, centrifuged for 5 min at 300 *g*, and resuspended in 1 mL of low-serum (5%, v/v, FBS) ECM. Next, cell suspensions (∼1.5 million cells per condition) were loaded in Oroboros Next Gen-O2K respirometry chambers (Oroboros Instruments, Innsbruck, Austria) after which the chambers were closed (1 mL chamber volume). Cells were allowed to reach equilibrium within 20 min before the start of the experiment. In serial order, oxygen ($O_2$) consumption was measured during basal respiration, complex V inhibition (5 µM ATP synthase blocker oligomycin, #O4876, Sigma-Aldrich), maximal respiration [6 µM carbonyl cyanide 4-(trifluoromethoxy) phenylhydrazone (FCCP uncoupler, #C2920, Sigma-Aldrich)], complex I inhibition (100 nM rotenone, #R8875, Sigma-Aldrich) and complex III inhibition (5 µM antimycin A, #A8674, Sigma-Aldrich). Data are corrected for cell count and

expressed as oxygen consumption rate (OCR) per pmol/s per cell. Spare capacity is calculated by subtracting the basal respiration from the maximal respiration, and expressed as a percentage (%) of the maximal respiration. The coupling efficiency is calculated as FCCP response, corrected for the leak respiration, as a percentage (%) to the maximal respiration.

### ATP measurement

Detection of total ATP was obtained with a CellTiter-Glo® 2.0 assay following the manufacturer's instructions (#G9241, Promega, Madison, WI, USA). Two micrograms of protein of each sample was analysed. Luminescence was detected (relative luminescence units) and quantified using a Spark® microplate luminescent reader (Tecan, Männedorf, Switzerland). Data are normalized to the experimental control.

### Mitochondrial membrane potential measurement

Mitochondrial membrane potential was measured with the fluorescent probe tetramethyl rhodamine methyl ester perchlorate (TMRM, #T5428, Sigma-Aldrich). Cells were incubated with TMRM (100 nM) for 20 min at 37°C in the dark. Subsequently, the excess of TMRM was washed away with serum-free ECM. Fluorescence was measured with a Biotek Synergy 4 plate reader (Agilent Technologies) at 548/574 excitation/emission. Data are normalized to the experimental control.

### SOD and catalase activity measurements

Total superoxide dismutase (SOD) activity was measured using the Superoxide Dismutase Activity Assay Kit (#ab65354, Abcam), assessing the repressing activity of xanthine oxidase by SOD. Catalase activity was assessed with the Catalase Activity Assay Kit (#ab83464, Abcam). Both assays were performed according to the manufacturer's instructions, and using the Spark microplate multimode reader (Tecan). The experimental control condition is set at 100%.

### mtDNA copy number

To isolate DNA for quantification of mtDNA copy number, cell pellets were lysed in 500 µL lysis buffer (100 mM Tris, 200 mM NaCl, 5 mM EDTA, pH 7.6) freshly supplemented with RNase (1 µg/mL) and Proteinase K (0.5 µg/mL) per millilitre of lysis buffer. Samples were incubated overnight at 56°C. Pellets were collected by centrifugation for 5 min at 12,000 *g* and 4°C. Samples were mixed with 400 µL isopropanol and DNA was precipitated. Subsequently, DNA was washed with 70% (v/v) EtOH three times and collected using centrifugation for 5 min at12,000 *g* and 4°C. Finally, DNA was solubilized in 250 µL Tris-EDTA and incubated at 56°C overnight. To quantify the mtDNA to nuclear DNA (nDNA) ratio, quantitative real-time PCR (qPCR) was performed with 10 ng DNA, Master Mix, GoTaq qPCR (#0000549407, Promega) and primers for NDUFA1 (for nDNA, sense 5′-CTGGCTACTGCGTACATCCA-3′, antisense 5′-ACCACCCTTTTCGGAAATCA-3′, Sigma-Aldrich) and mtND1 (for mtDNA, sense 5′-TGGCTCCTTTAACCTCTCCA-3′, antisense 5′-GGTTCGGTTGGTCTCTGCTA-3′, Sigma-Aldrich). Differences in mtDNA copy number were calculated by the $^{\Delta\Delta}$Ct method, where $^{\Delta}Ct = Ct_{mtND1} - Ct_{NDUFA1}$, and $^{\Delta\Delta}Ct = {}^{\Delta}Ct_{(\text{sample of interest})} - \Sigma^{\Delta}Ct_{(\text{control samples})}$, after which relative expression levels towards the experimental control were calculated ($2^{\wedge}$-$^{\Delta\Delta}$Ct).

### Mitochondrial network visualization and quantification

To visualize and quantify mitochondrial networks, ECs were cultured on coverslips, and incubated with MitoTracker™ Deep Red FM (200 nM, #M22426, ThermoFisher Scientific), for 30 min at 37°C in the dark. Coverslips were washed with PBS and fixed in 2% (w/v) PFA. Coverslips were placed on StarFrost Microscope slides using Aqua-Poly/Mount mounting medium. Mitochondrial networks were visualized with a confocal laser scanning microscope (Leica TCS SP8) using a 63× objective, and analysed with the ImageJ software (v.2.14.0/1.54f) (Schneider et al., 2012), using the DeconvolutionLab2, PSF generator and Mitochondrial Analyzer plugin. Data are normalized to the experimental control.

### Cell viability assay

To measure cell viability after CPP exposure, a Neutral Red Toxicity Assay was performed. Cells were first stimulated with CPPs, in the absence or presence of cyclosporin A (CSA, mitochondrial permeability transition pore (mPTP) inhibitor, 10 nM to 1 µM, #S2286, SellekChem, Houston, TX, USA) or Ru265 (inhibitor of the mitochondrial calcium uniporter (MCU), 12.5–50 µM Ru265, kindly provided by Prof. A. M. Dolga, Dept. of Molecular Pharmacology, UMCG, the Netherlands) for 24 h, after which cells were incubated with Neutral Red (0.33% in culture medium (w/v), #N4638, Sigma-Aldrich) for 2 h at 37°C. Next, cells were washed twice with PBS and incubated with NRU solubilize solution (1% acetic acid, 50% EtOH in demi-$H_2O$ (v/v)) for 15 min

ar room temperature. Absorbance of the Neutral Red was measured at 540 nm. Absorbance was corrected for background signal at 690 nm. Data are normalized to the experimental control.

### NanoString gene expression analysis

To assess possible altered gene expression patterns of ECs exposed to CPPs ± CSA, RNA from the stimulated ECs was subjected to NanoString gene expression analysis, using the nCounter® CVD Pathophysiology Panel (NanoString Technologies, Seattle, WA, USA). First, total RNA was extracted using a RNeasy® Mini kit (#74106, Qiagen, Venlo, the Netherlands) and RNA integrity and quantification were determined using both the Nanodrop spectrophotometer and Qubit Fluorometer (ThermoFisher Scientific). Next, 100 ng RNA was added to hybridization buffer and a reporter probe. After briefly spinning down, the capture probe was added, and the mixture was incubated for hybridization at 65°C for 16 h. Digital data acquisition of the hybridized mixture was performed in the nCounter Prep Station and Digital Analyzer (NanoString Technologies). The nCounter cartridge was scanned at 555 fields of view to identify unique barcodes. Raw data were analysed using nSolver 4.0 and NanoString ROSALIND (version 3.37.6.11). Thresholds were set at a fold change of $\leq -1.5$ or $\geq 1.5$ and adjusted $P < 0.05$. Gene enrichment analysis for EC function was performed with gene set analysis with NanoString Annotations v46, using the directed global significance score. Raw data underlying the NanoString analysis of this study will be available upon reasonable request to the corresponding author.

### Statistics

Statistical analyses were performed with GraphPad Prism 10.0.3 (GraphPad Software Inc., Boston, MA, USA). Raw data were normalized to the experimental control by dividing the raw data value of each sample by the average value of all experimental control samples. Individual normalized samples are plotted. Normality tests were run for all experiments. Differences between the two groups were tested with the non-parametric Mann–Whitney U test. Differences between three or more experimental groups were tested with a non-parametric Kruskal–Wallis test using Dunn's test for multiple comparisons or ordinary two-way ANOVA using Šidák's *post hoc* test for multiple comparisons. Data are presented as median ± interquartile range (IQR). Graphs were generated with GraphPad Prism and multi-panel figures were composed with Adobe Illustrator 27.7 (Adobe Inc., San Jose, CA, USA).

## Results

### CPPs increase both the cytosolic and mitochondrial calcium concentration

We examined the impact of CPP exposure on both cytosolic and mitochondrial calcium ($Ca^{2+}$) levels. When ECs were exposed to CPPs (50 µg/mL, 24 h), a clear increase in cytosolic $Ca^{2+}$ levels could be observed compared to the unstimulated control condition (Fig. 1*A*, green signal). A similar increase was found for mitochondrial $Ca^{2+}$ levels, which were higher in the ECs exposed to CPPs compared to unstimulated ECs (Fig. 1*C*, red signal). Quantification of both the cytosolic and mitochondrial $Ca^{2+}$ signals confirmed the visual observations and showed a significant increase in both cytosolic and mitochondrial $Ca^{2+}$ levels as a result of CPP exposure (Fig. 1*B* and *D*).

### Dysregulated calcium ion homeostasis in ECs after CPP exposure

To identify pathways in ECs which are affected by CPPs, proteome analysis was performed. In total, 8092 proteins were identified, of which 7936 (98.1%) were shared among the control and CPP-exposed ECs, 117 (1.4%) were found only in ECs under control conditions, and 39 (0.5%) were exclusively present in ECs stimulated with CPPs (Fig. 2*A*). Using an FDR-adjusted $P < 0.05$ and $\log_2$ fold change $>0.58$ and $<-0.58$, we found 103 proteins with differential abundance in the CPP-exposed ECs (29 with increased and 74 with decreased abundance), compared to the unstimulated controls (Fig. 2*B*, red dots). Enrichment analyses of differentially abundant proteins for biological processes, molecular function and cellular compartment identified a differential abundance of proteins involved in cartilage and connective tissue development, and collagen biosynthesis, and confirmed enrichment of proteins involved in calcium ion binding, glycosaminoglycan and heparin binding within the extracellular matrix and ER (Fig. 2*C*). Unexpectedly, no specific enrichment for mitochondrial proteins was found for differentially abundant proteins.

As no specific pathways explaining the cytoplasmic or mitochondrial calcium infux were identified, we continued to specifically analyse alterations in calcium-related pathways in ECs. Here, 1.8% of the identified proteome overlapped with proteins included in a manually curated list of calcium-related gene ontology pathways (see Methods for details) (Fig. 3*A*). Additionally, seven proteins were differentially abundant within the CPP-exposed ECs, compared to the unstimulated controls (Fig. 3*B*; red dots). Pathways related to vitamin D responses and metabolic processes were significantly enriched in CPP-exposed ECs, whereas pathways related

to intracellular calcium homeostasis were enriched in unstimulated control ECs (Fig. 3*C*). Subcellular location analysis showed a significantly reduced enrichment of ER calcium ion homeostasis of ECs after CPP exposure, but enrichment of mitochondrial and cytosolic calcium homeostasis was not found (Fig. 3*D*). These data indicate that CPPs decrease the abundance of proteins involved in the pathways of calcium metabolism of the ER, which might affect the intracellular cellular calcium homeostasis of the CPP-exposed ECs.

## Impaired OXPHOS signalling in ECs after CPP exposure

As we confirmed CPP-induced changes in pathways associated with calcium homeostasis, but not with mitochondrial calcium uptake, we analysed if downstream mitochondrial processes might be affected and performed targeted pathway enrichment using the MitoCarta v3.0 dataset on the complete proteome dataset. In total, 9.7% of the identified proteome overlapped with proteins in the MitoCarta v3.0 dataset (Fig. 4*A*). Additionally, five mitochondria-related proteins were differentially abundant in response to CPP exposure (Fig. 4*B*; red dots). When comparing different mitochondrial compartments between groups, a significantly decreased enrichment of MIM proteins was observed in the CPP-exposed ECs, compared to unstimulated controls (Fig. 4*C*). Furthermore, process-specific alterations were observed within OXPHOS, where significantly reduced enrichment was found in the CPP-exposed ECs compared to the unstimulated controls (Fig. 4*D*). In contrast, pathways involved in, for example, mitochondrial

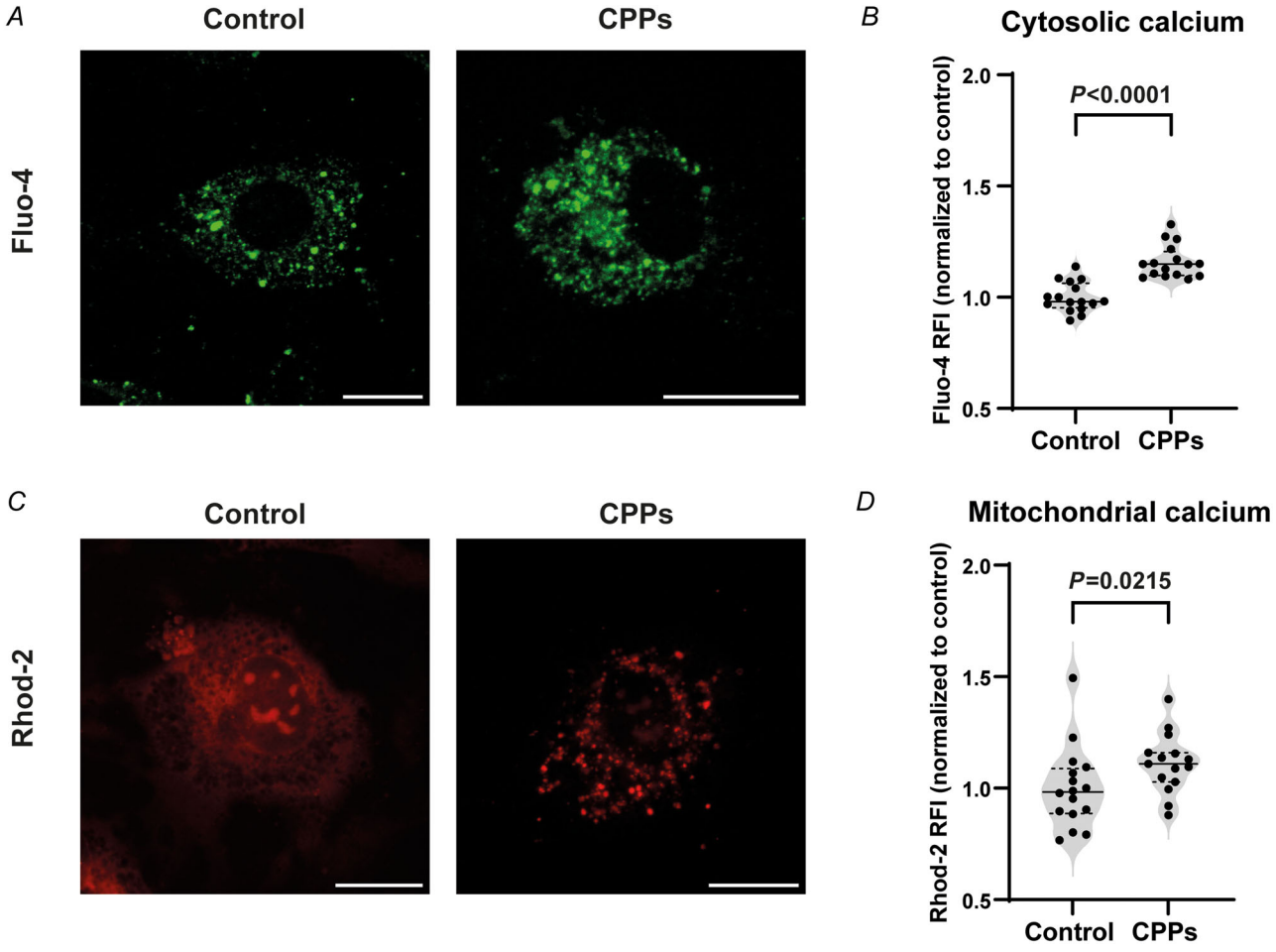


**Figure 1. Cytosolic and mitochondrial calcium increase upon CPP exposure**
*A*, immunofluorescence images of cytosolic $Ca^{2+}$ in CPP-exposed endothelial cells or control. *B*, quantification of cytosolic $Ca^{2+}$ in ECs. *C*, immunofluorescence images of mitochondrial $Ca^{2+}$ in CPP-exposed ECs or control. *D*, quantification of mitochondrial $Ca^{2+}$ in ECs. Data are presented as median ± IQR with individual data points and normalized to the experimental control ($n$ = 16, derived from four individual experiments). $P < 0.05$ is considered statistically significant and tested with Mann–Whitney U test. Exact *P*-values are indicated in the graphs. Scale bar represents 20 µm.

dynamics, signalling or small molecule transport were not (significantly) altered. Within the OXPHOS complexes, complexes I–III and the OXPHOS subunits were significantly enriched in unstimulated controls as compared to CPP-stimulated ECs (Fig. 4*E*).

Each OXPHOS complex comprises many different subunits (Alam et al., 2016). To assess OXPHOS-specific protein alterations within the ECs, western blot analysis for complexes I–V was performed (Fig. 5). For this analysis, a specific cocktail of antibodies was used to detect one subunit of each complex (NDUFB8 for complex I, SDHB for complex II, UQCRC2 for complex III, MTCO1 for complex IV and ATP5A for complex V). No significant alterations in protein expression were observed for the specific subunits of complexes I–III. Combining proteome data and western blot analysis suggests that the protein abundance of several subunits of complexes I–III was altered, while other proteins in the same complex were unaffected.

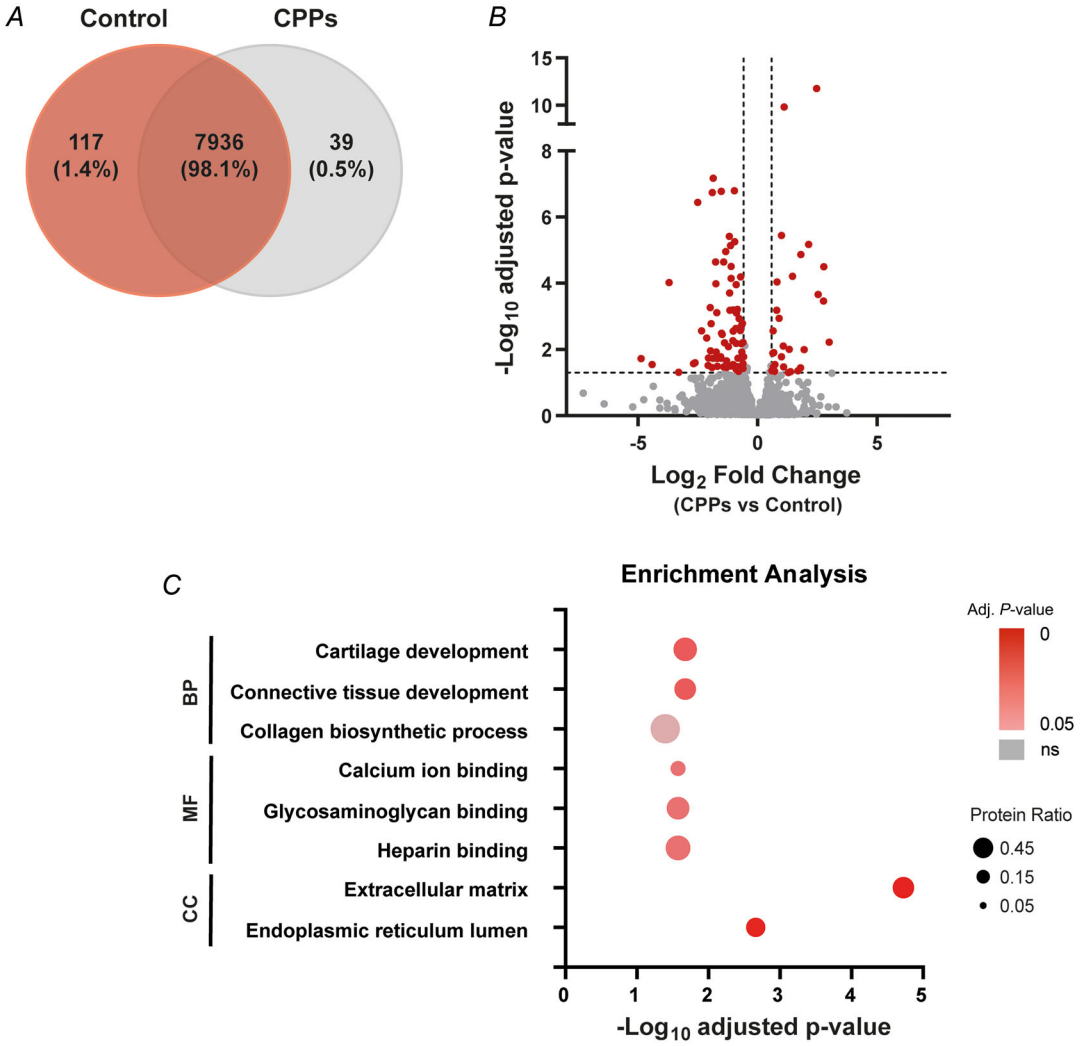


**Figure 2. General characteristics of the cellular proteome analysis**
*A*, Venn diagram showing the number and percentage (%) of proteins in the total proteomics dataset and per group (control or CPP-exposed ECs). *B*, volcano plot showing differentially expressed proteins (indicated in red) between ECs stimulated with CPPs or unstimulated controls with cut-off values of FDR-adjusted $P < 0.05$ and $\log_2$ fold change >0.58 and <−0.58. *C*, bubble plot showing enrichment analysis for biological processes (BP), molecular function (MF) and cellular compartment (CC) in the total proteomics dataset. Cut-off values of FDR-adjusted $P < 0.05$ are considered significant. Significant processes are indicated with a red gradient. Non-significant processes are indicated in grey (ns). The $-\log_{10}$ adjusted *P*-value is indicated on the *x*-axis and the size of the dots indicates the protein ratio (i.e. fraction of differently expressed proteins of the total dataset). Data are based on $n = 4$ samples per group, derived from two individual experiments.

### CPPs impair mitochondrial respiration, increase ATP production and affect the antioxidant capacity

To assess whether CPPs affect mitochondrial respiration, high-resolution respirometry was performed (Fig. 6*A*). Basal and maximal respiration were reduced in CPP-exposed ECs (Fig. 6*B* and *C*) compared to the unstimulated condition. Mitochondrial spare capacity [i.e. the difference between maximal and basal respiration in relation to maximal respiration (%)] was not altered (Fig. 6*D*). Both CPP-stimulated ECs and unstimulated ECs (control) consumed equal amounts of oxygen ($O_2$) for ATP production, as indicated by the coupling efficiency (Fig. 6*E*). Surprisingly, when measuring ATP production in both groups, a significant increase was observed after CPP exposure, compared to the unstimulated control (Fig. 6*F*). Furthermore, the mitochondrial membrane potential was significantly decreased in ECs after CPP exposure (Fig. 6*G*). Results were comparable to ECs exposed to the ETC uncoupler FCCP, which served as a positive control for membrane potential deterioration. Additionally, our previous data showed that mitochondrial-derived superoxide ($O_2^{\cdot -}$) levels are elevated in ECs after CPP stimulation, resulting in peroxynitrite ($ONOO^-$) formation and subsequent protein damage of ECs (Feenstra et al., 2023). When

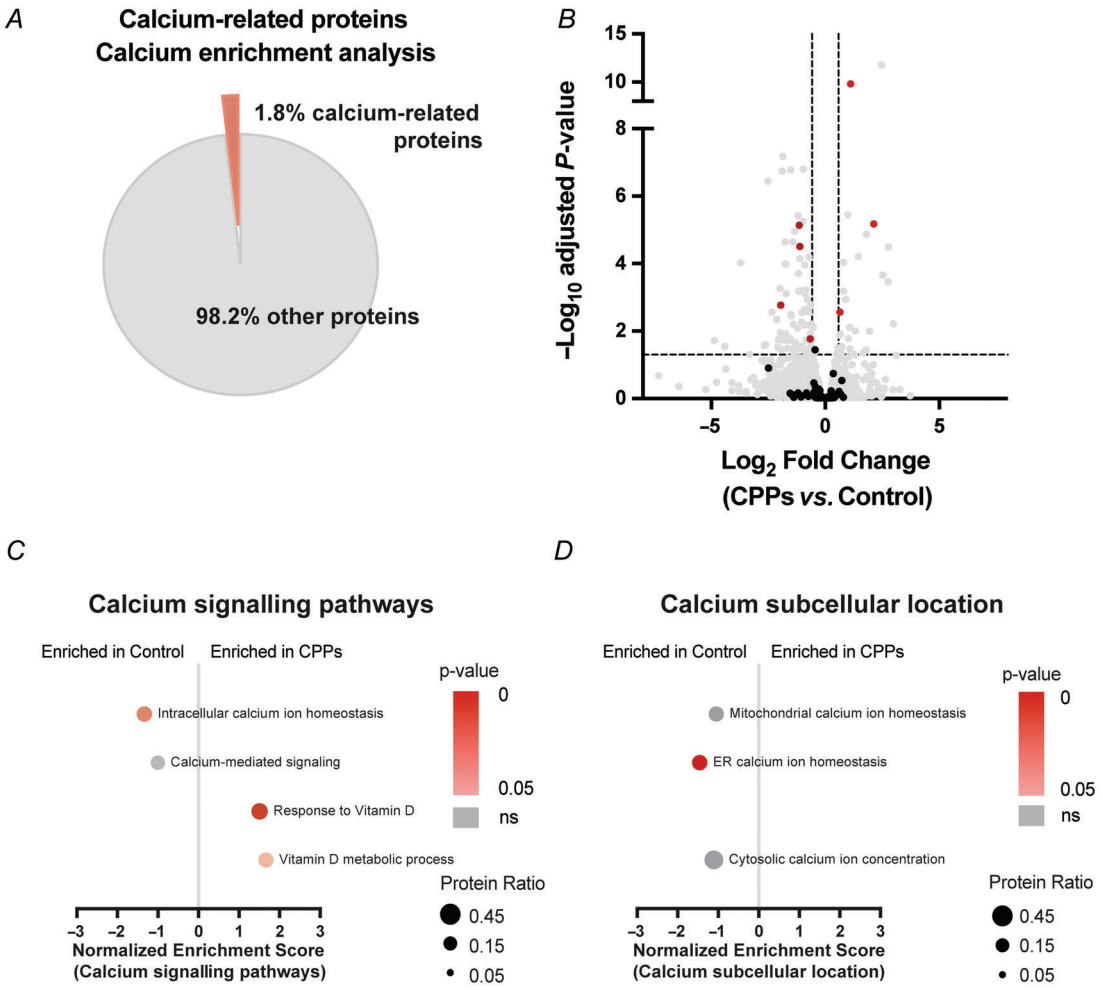


**Figure 3. EC proteome analysis: calcium-related pathways**
*A*, pie chart showing the percentage (%) of calcium-related proteins in the proteomics dataset. *B*, volcano plot showing differentially expressed proteins (indicated in red) between ECs stimulated with CPPs or unstimulated control ECs with cut-off values of FDR-adjusted $P < 0.05$ and $\log_2$ fold change $>0.58$ and $<-0.58$. Grey dots indicate all proteins detected in the complete proteome dataset. Black dots indicate the proteins detected in the specific calcium-related dataset. *C* and *D*, bubble plots showing calcium signalling pathways (*C*) and calcium subcellular location (*D*) of the proteomics dataset. Cut-off values of $P < 0.05$ are considered significant. Significant processes are indicated with a red gradient. Non-significant processes are indicated in grey (ns). The normalized enrichment score of the bubble plots is indicated on the *x*-axis and the size of the dots indicates the protein ratio (i.e. fraction of differently expressed proteins of the total dataset). Data are based on the proteome analysis of $n = 4$ samples per group derived from two individual experiments.

analysing SOD and catalase activity in ECs exposed to CPPs, reduced activity of both total SOD and catalase was observed, indicating impaired antioxidant capacity in CPP-exposed ECs (Fig. 6*H* and *I*). Collectively, these data demonstrate that CPPs not only affect EC antioxidant capacity but also mitochondrial respiration and mitochondrial membrane potential, all contributing to impaired mitochondrial function.

## Reduced mtDNA copy number and mitochondrial network integrity in CPP-stimulated ECs

Next, we investigated whether a decreased mitochondrial respiration can be attributed to possible decreases in the numbers of mitochondria (based on mtDNA copy number) and/or deterioration of the mitochondrial network. Quantification of the mtDNA content (corrected for total nDNA content) showed a 2-fold reduction in mtDNA copy numbers within CPP-exposed ECs, compared to the unstimulated controls (Fig. 7*A*). To analyse the integrity of the mitochondrial network, MitoTracker Deep Red staining was used (Fig. 7*B*). CPPs significantly affected mitochondrial network integrity by increasing the number of branch end points and branch junctions (Fig. 7*C* and *D*), without affecting the total number of branches (Fig. 7*E*). These data indicate that CPPs reduce the mtDNA copy number, and thereby numbers of mitochondria, and cause disintegration of the mitochondrial network in ECs.

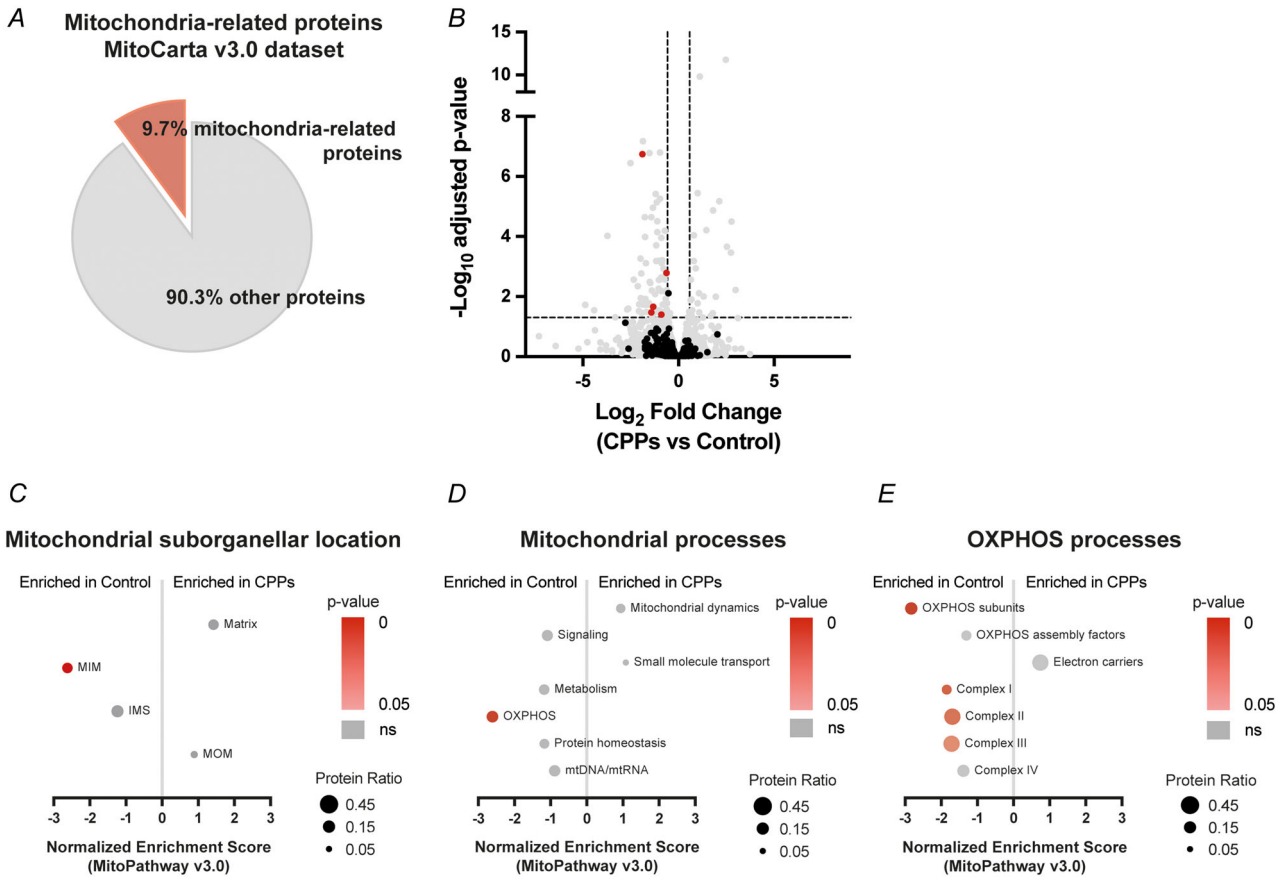


**Figure 4. EC proteome analysis: mitochondria-related pathways**
*A*, pie chart showing the percentage (%) of mitochondria-related proteins in the proteomics dataset. *B*, volcano plot showing differentially expressed proteins (indicated in red) between ECs stimulated with CPPs or unstimulated controls with cut-off values of FDR-adjusted $P < 0.05$ and $\log_2$ fold change $>0.58$ and $<-0.58$. Grey dots indicate all proteins detected in the complete proteome dataset. Black dots indicate the proteins detected in the specific MitoCarta dataset. *C*–*E*, bubble plots showing protein enrichment of mitochondrial location (*C*), mitochondrial processes (*D*) and oxidative phosphorylation (OXPHOS)-related specific processes (*E*) of the proteomics dataset, using cut-off values of $P < 0.05$ as significant. Significant processes are indicated with a red gradient. Non-significant processes are indicated in grey (ns). The normalized enrichment score of the bubble plots is indicated on the *x*-axis and the size of the dots indicates the protein (i.e. fraction of differently expressed proteins of the total dataset). Data are based on the proteome analysis of $n = 4$ samples per group derived from two individual experiments.

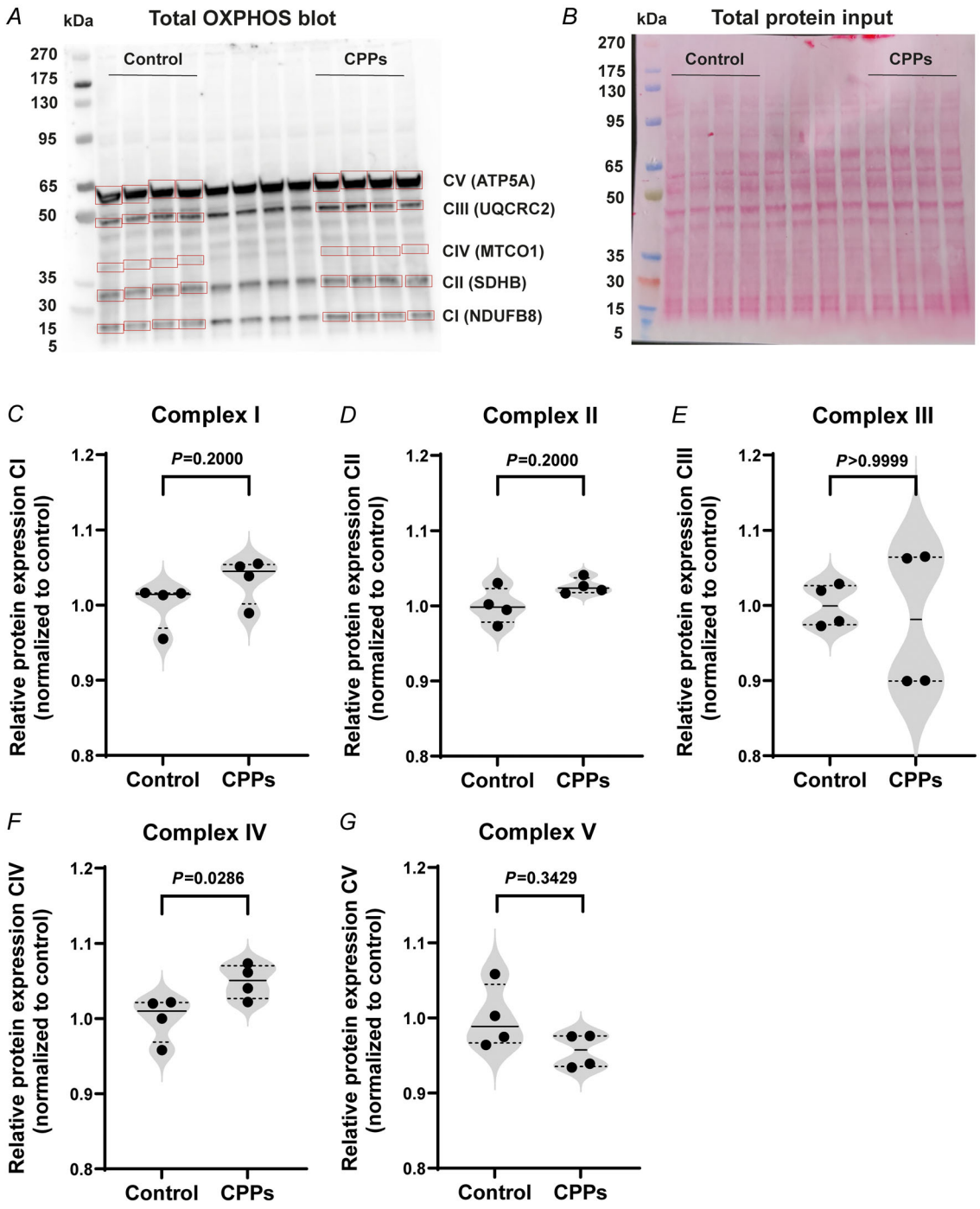


**Figure 5. Immunoblotting of OXPHOS complexes of CPP-exposed ECs**
*A*, immunoblot for OXPHOS complexes I–V (NDUFB8 for complex I, SDHB for complex II, UQCRC2 for complex III, MTCO1 for complex IV and ATP5A for complex V). *B*, Ponceau S staining for all OXPHOS complexes (input reference blot). Numbers on the left side of the blot indicate molecular weight (kDa) and abbreviations on the right side of the blot indicate the different OXPHOS complexes. *C–G*, quantification of protein expression of OXPHOS complexes I–V of ECs exposed to CPPs and controls. Data are presented as median ± IQR with individual data points and normalized to the experimental control. Data are based on $n = 3–4$ samples per group derived from two individual experiments. $P < 0.05$ is considered significant and tested with Mann–Whitney U test. Exact *P*-values are indicated in the graphs.

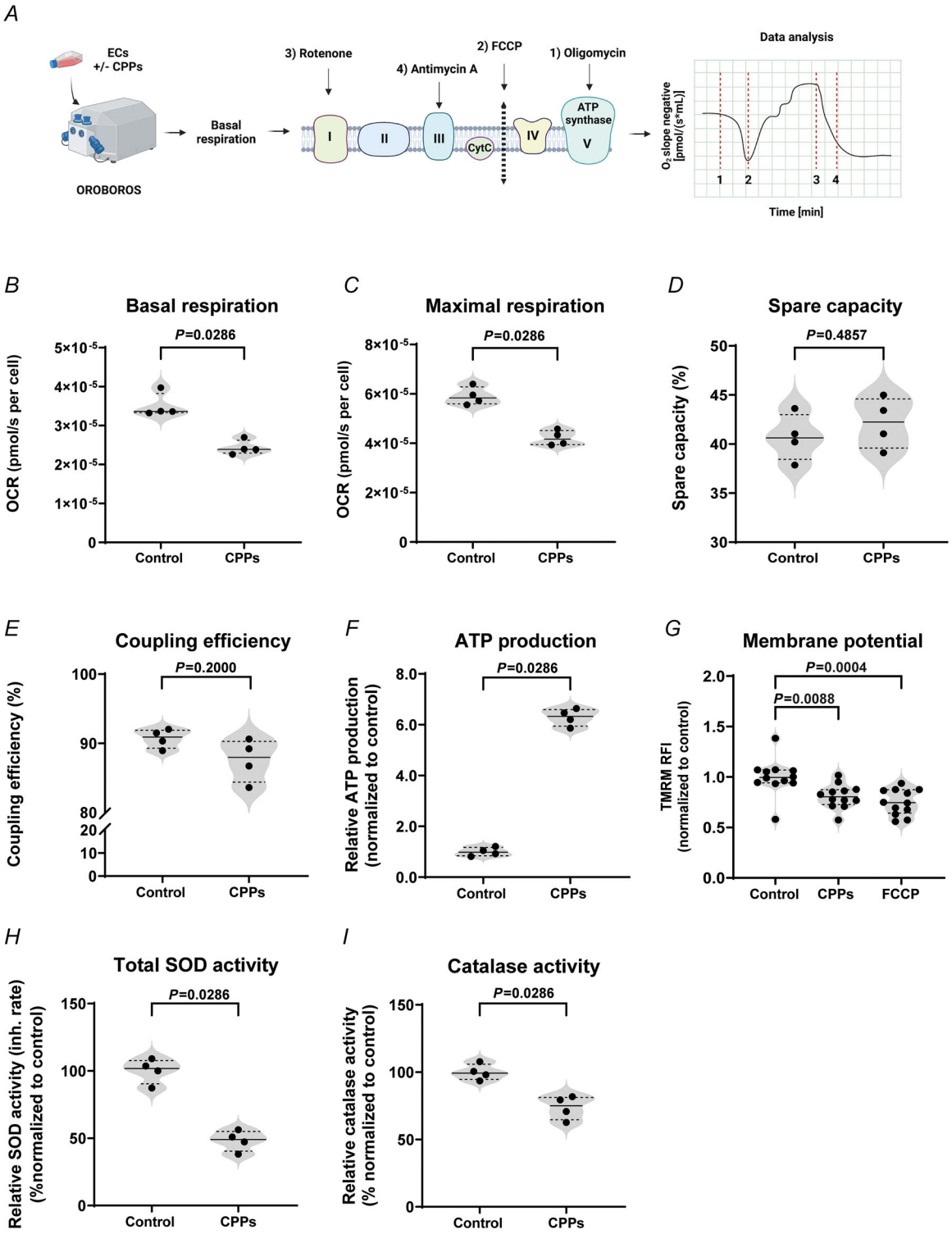


**Figure 6. Mitochondrial respiration, membrane potential and antioxidant capacity of ECs after CPP exposure**

*A*, overview of the high-resolution respirometry experimental set-up and measurements. *B*–*E*, high-resolution respirometry data showing basal respiration (*B*), maximal respiration (*C*), spare capacity (*D*) and the coupling efficiency (*E*) in ECs stimulated with CPPs or unstimulated controls. Data are presented as median ± IQR with individual data points (pmol/s per cell) or shown as a percentage (%) of the maximal respiration. *F*, ATP production of ECs. *G*, mitochondrial membrane potential in CPP-exposed ECs or unstimulated controls. FCCP uncoupler is used as a positive control. *H* and *I*, total superoxide dismutase (SOD) (*H*) or catalase (*I*) activity in ECs stimulated

with CPPs or unstimulated controls. Inh. rate (panel H) = inhibition rate. Data are presented as median ± IQR with individual data points or shown as a percentage (%) ($n$ = 4–12 samples, derived from two to four individual experiments). *F–I* are normalized to the experimental control. $P < 0.05$ is considered significant and tested with Mann–Whitney U test or Kruskal–Wallis test with Dunn's multiple comparisons. Exact *P*-values are indicated in the graphs.

## Blocking opening of the mPTP prevents CPP-induced endothelial activation and improves viability

Opening of the mPTP is a key factor in driving mitochondrial dysfunction (Feno et al., 2019; Matuz-Mares et al., 2022). We therefore evaluated whether the presence of CSA, a mPTP opening blocker, was able to improve cell viability after exposure of ECs to CPPs. CSA supplementation indeed significantly increased cell viability after CPP exposure causing restoration to control (i.e. no CPP exposure) levels (Figs 8*A* and 9*A*). Unlike CSA, Ru265 (i.e. an inhibitor of the MCU on the MIM and blocker of $Ca^{2+}$ influx into the mitochondrial matrix) did not improve but rather worsened cell viability (Fig. 8*B*).

To further analyse the underlying molecular pathways of the observed protective effects of CSA, NanoString gene expression analysis on CPP-exposed ECs in the presence or absence of CSA was performed. Principal component analysis (PCA) showed that each group (±CPPs, ±CSA) exhibited a unique gene expression pattern (Fig. 9*B*). Additionally, the data showed that ECs exposed to both CPPs and CSA cluster more closely with the unstimulated ECs (control), compared to the ECs treated with CPPs only. When first comparing unstimulated ECs

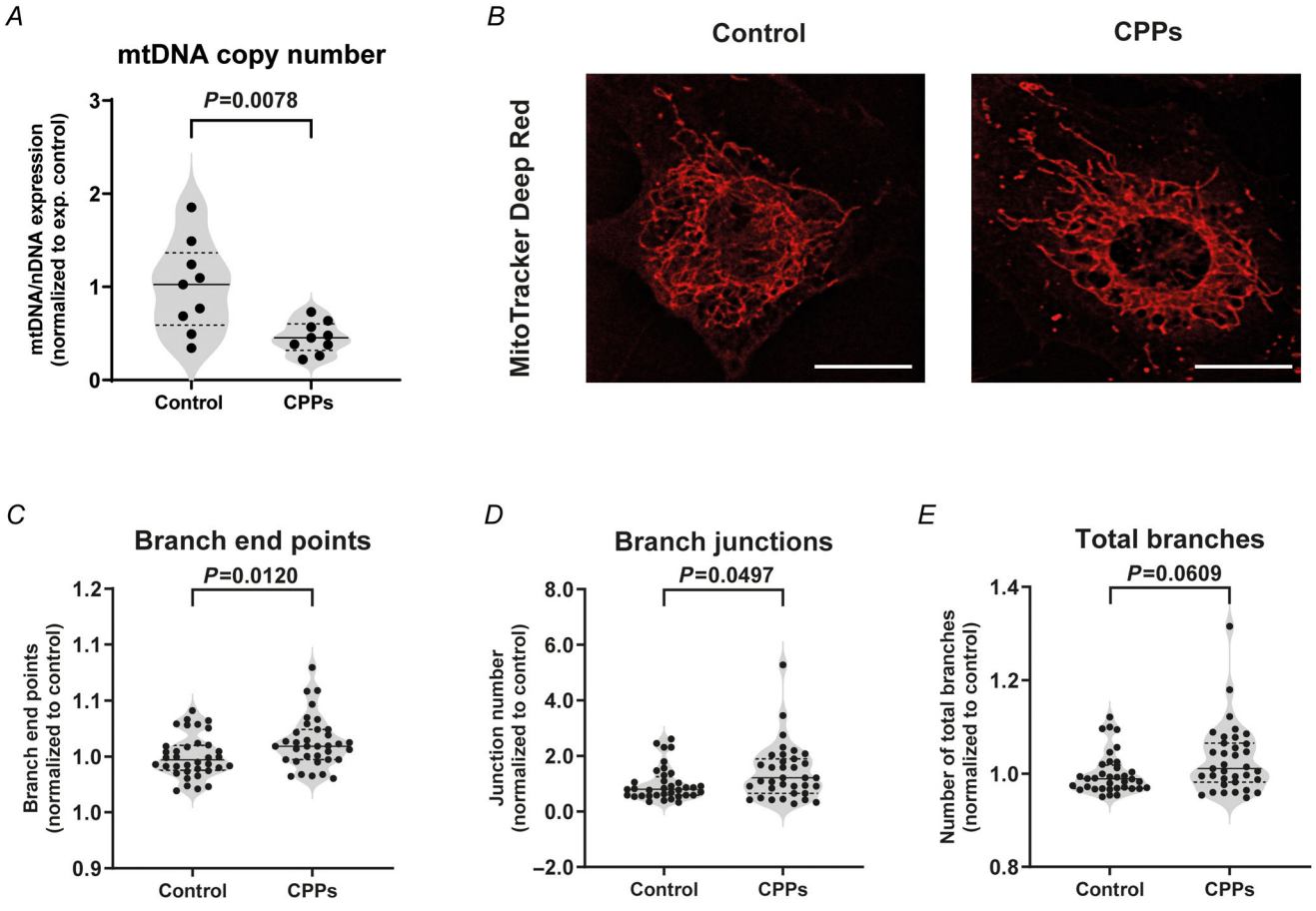


**Figure 7. Mitochondrial copy number and network integrity of CPP-exposed ECs**
*A*, mtDNA quantification in ECs stimulated with CPPs or unstimulated controls [ratio to nuclear (n)DNA]. *B*, immunofluorescence images of MitoTracker Deep Red in ECs (control *vs*. CPP stimulated). Scale bar represents 20 µm. *C–E*, quantification of mitochondrial network integrity by measuring branch end points (*C*), branch junctions (*D*) and total branches (*E*) in ECs after CPP exposure. Data are presented as median ± IQR with individual data points and normalized to the experimental control ($n$ = 9 for mtDNA quantification and $n$ = 35–36 cells for MitoTracker staining, derived from three individual experiments). $P < 0.05$ is considered significant and tested with Mann–Whitney U test. Exact *P*-values are indicated in the graphs.

with CPP-exposed ECs (both without CSA), 40 genes were differentially expressed (Fig. 9*C*, red dots). A list of differentially expressed genes of both comparisons (Fig. 9*C* and *D*) can be found in Table S1. CPP stimulation in the presence of CSA resulted in significant differential expression of 23 genes compared to the CPP-exposed ECs without CSA (Fig. 9*D*, red dots). To evaluate if CSA treatment would improve the CPP-induced alterations in gene expression, fold changes of CPPs *vs*. Control (without CSA) were compared to CPPs + CSA *vs*. Control, in a two-dimensional Volcano plot. Differentially expressed genes between CPPs + CSA *vs*. CPPs are indicated in red (Fig. 9*E*). Considering our interest in EC function, we labelled (i.e. added gene name) the differentially expressed genes that are related to EC activation and inflammation (Fig. 9*E*). The normalized mRNA counts of these genes are depicted in Fig. 9*F*–*I*. For the genes ICAM-1 (endothelial activation marker), chemokine (C-C motif) ligand 2 (CCL2), chemokine (C-X-C motif) ligand 8 (CXCL8) (chemokines) and caveolin-1 (inflammatory marker), an increased expression in ECs after CPP exposure was found. Administration of CSA significantly reduced the expression of these genes (Fig. 9*F*–*I*).

To gain further insight into pathways affected by CPPs, and possibly rescued by CSA, gene set enrichment analysis was performed (i.e. CPPs *vs*. control, or CPPs + CSA *vs*. control) using NanoString annotations (Fig. 9*J*). Enrichment was found for various signalling pathways including toll-like receptor (TLR), nuclear factor kappa B (NF-$\kappa$B) and IL-6 signalling, comparing CPP-exposed ECs to unstimulated ECs. This enrichment was reduced in cells exposed to CPPs in the presence of CSA. In contrast, processes such as VEGF and calcium signalling, lipoprotein clearance and integrin signalling were reduced in ECs after CPP stimulation (compared to unstimulated ECs). CSA administration reversed these effects, and induced enrichment of these pathways, compared to the control. Combined, these data indicate that CSA rescues ECs from the CPP-induced activation and inflammatory signalling.

## Discussion

Endothelial activation and dysfunction are considered the instigators of the development of cardiovascular diseases (Medina-Leyte et al., 2021; Sun et al., 2020). CPPs seem to be involved in the development of VC in CKD, but the underlying mechanisms are largely unknown, in particular, the role ECs have in this process. CPPs have been shown to activate ECs *in vitro* (Shishkova et al., 2021; Thiem et al., 2023), and we recently showed CPPs uncoupled eNOS resulting in EC dysfunction (Feenstra et al., 2023). To further explore the role of mitochondria in the aforementioned CPP-mediated effects on ECs, here we investigated whether CPPs affect mitochondrial function, the underlying molecular pathways, and whether mitochondria can serve as a therapeutic target. We showed that exposure of ECs

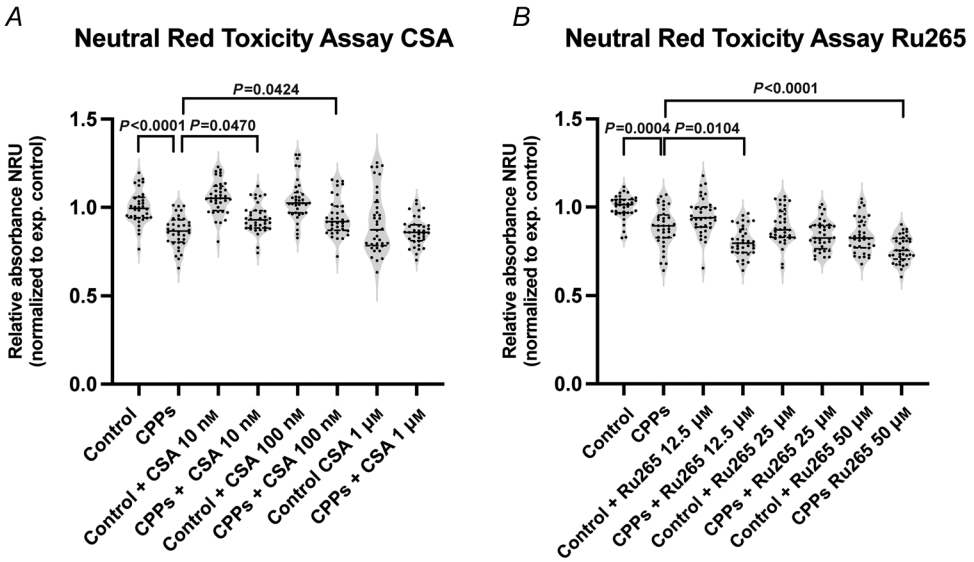


**Figure 8. Neutral Red toxicity assay: dose–response effects on cell viability of CSA and Ru265 on CPP-exposed ECs**
*A* and *B*, Neutral Red toxicity assay of ECs exposed to CPPs in the presence of cyclosporin A (CSA) (*A*) or Ru265 (*B*). Data are presented as median ± IQR with individual data points and normalized to the experimental control [$n$ = 36 samples, derived from three individual (96-well plate) experiments, 1 well = 1 data point]. $P < 0.05$ is considered significant and tested with Kruskal–Wallis test and Dunn's test for multiple comparisons. Exact $P$-values are indicated in the graphs.

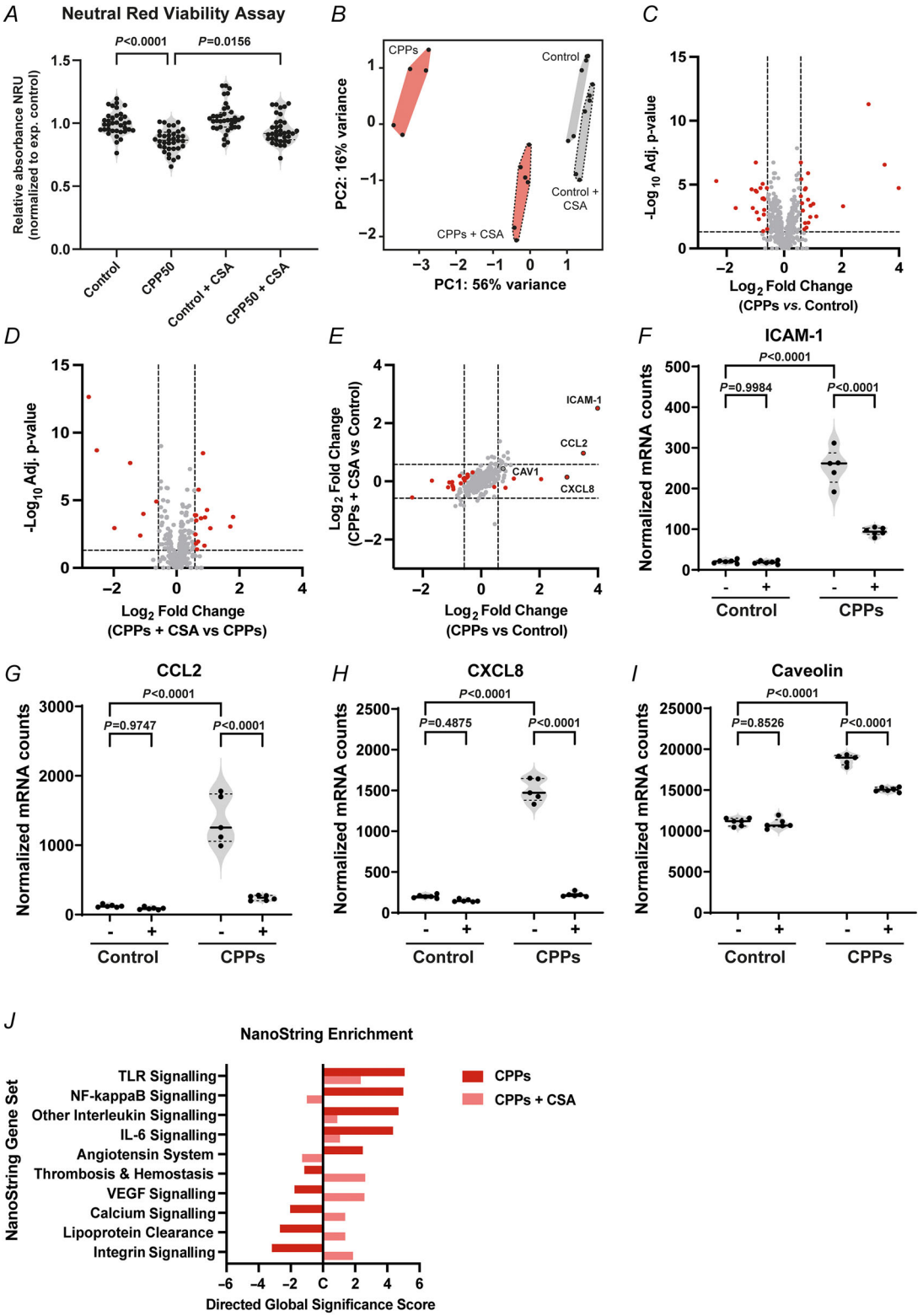


**Figure 9. Cyclosporin A intervention, endothelial viability and NanoString enrichment analysis in CPP-exposed ECs**

*A*, Neutral Red toxicity (cell viability) assay of ECs exposed to CPPs in the presence or absence of cyclosporin A (CSA, 100 nM). Data are presented as median ± IQR with individual data points and normalized to the experimental control [*n* = 36 derived from three individual (96-well plate) experiments, 1 well = 1 data point]. *B*, principal component analysis (PCA) of experimental groups included in NanoString analysis. Groups with CSA treatment

are indicated as clusters surrounded by a black dashed line. Clusters of CPP-exposed ECs are indicated in pink, and control (non-exposed ECs) in grey. *C*, volcano plot showing differentially expressed genes in CPP-exposed ECs compared to controls (non-exposed ECs). *D*, volcano plot showing differentially expressed genes in CPP-exposed ECs with CSA compared to CPP-exposed ECs without CSA treatment. Significant differentially expressed genes are indicated in red. *E*, two-way volcano plot showing relationship of fold changes between CPP-exposed and control ECs on the *x*-axis, and CPP-exposed + CSA-treated ECs *vs*. control ECs on the *y*-axis. Differentially expressed genes between CPP-exposed ECs with and without CSA treatment are indicated in red. A subset of genes related to EC activation and inflammation is indicated with a label and black border surrounding the dot. All volcano plots include cut-off values of FDR-adjusted $P < 0.05$ and $\log_2$ fold change $>0.58$ and $<-0.58$. *F–I*, ICAM-1 gene expression (*F*), CCL2 gene expression (*G*), CXCL8 gene expression (*H*) and Caveolin-1 (CAV1) gene expression (*I*) for control ECs and CPP-exposed ECs, with and without CSA treatment. Data are shown as median ± IQR and individual data points ($n$ = 5–6 samples, derived from three individual biological experiments). *J*, enrichment analysis using the NanoString Annotations database. Enriched gene sets are shown on the *y*-axis. The Directed Global Significance Score is shown on the *x*-axis. Enrichment is indicated for both CPP-exposed ECs with or without CSA treatment, in comparison to the control ECs (without CSA) indicated with '*C*'. $P < 0.05$ is considered significant and tested with a Kruskal–Wallis test and Dunn's multiple comparisons (*A*) or ordinary two-way ANOVA with Šidák's *post hoc* test (*F–I*). Exact *P*-values are indicated in the graphs.

to CPPs induces $Ca^{2+}$ overload, which is associated with loss of mitochondria and mitochondrial dysfunction culminating in EC activation and cell loss. Targeting mitochondria with CSA attenuated CPP-induced EC activation and cell loss.

Exposure of ECs to CPPs *in vitro* led to an increase in both cytosolic and mitochondrial calcium ($Ca^{2+}$) concentrations. Enrichment analysis of the cellular proteome data indicated a decreased abundance of proteins involved in intracellular $Ca^{2+}$ homeostasis, which could mainly be attributed to a decreased abundance of proteins regulating ER ion $Ca^{2+}$ homeostasis, while no significant differences were observed in mitochondrial $Ca^{2+}$ regulating proteins. Intracellularly, the ER and Golgi apparatus are the main organelles responsible for $Ca^{2+}$ homeostasis, while the mitochondria take up $Ca^{2+}$ from the cytosol during steep increases of intracellular $Ca^{2+}$, and function mainly as buffering organelles (Panda et al., 2021). It could be hypothesized that because of CPP exposure and endocytosis, cytosolic $Ca^{2+}$ concentrations rise, leading to $Ca^{2+}$ uptake in the ER. Under conditions of stress, local efflux of $Ca^{2+}$ from the ER can modulate the distance of mitochondria towards the ER (Bravo et al., 2011; Rossi et al., 2019). In response to increasing $Ca^{2+}$concentrations, mitochondria can come into close proximity to the ER, leading to $Ca^{2+}$ uptake in the mitochondrial matrix (Bravo et al., 2011; Deniaud et al., 2008; Rossi et al., 2019).

Mitochondria can regulate high matrix $Ca^{2+}$ concentrations via the opening and closing of the mPTP. In conditions of $Ca^{2+}$ overload, the mPTP is formed and opened permanently creating a permeable state in which molecules can flow in and out of the mitochondria, and where the membrane potential decreases considerably (Brookes et al., 2004; Rossi et al., 2019; Zhou et al., 2022). Due to the loss of membrane potential, respiratory capacity and ATP production deteriorate (Elustondo et al., 2016; Feno et al., 2019). CPP exposure resulted in both cytosolic and mitochondrial calcium overload. This was accompanied by reduced mitochondrial basal respiration and maximal respiration, with preserved spare capacity and coupling efficiency. Moreover, the mitochondrial membrane potential decreased significantly in response to CPP exposure. Our proteome data supported these findings by showing a decreased abundance of proteins involved in OXPHOS, especially complexes I–III, indicating respiratory dysfunction. Collectively these data indicate that CPPs reduce mitochondrial respiration and function, probably as a consequence of mitochondrial $Ca^{2+}$ overload.

CPP exposure resulted in increased ATP production which was rather unexpected since reduced mitochondrial respiration is associated with reduced mitochondrial ATP production. The observed increase in ATP might be due to the fact that ECs are known to mainly produce ATP via glycolysis, in contrast to many other cell types (Li et al., 2022). Additionally, in activated ECs, glycolysis is increased in order to meet the energy demand in the activated pro-inflammatory state (Schnitzler et al., 2020), a process counteracted by increasing OXPHOS (Xiao et al., 2021). We showed that exposure of ECs to CPPs indeed results in activation, as demonstrated previously by others (Kutikhin et al., 2016; Thiem et al., 2023). Therefore, despite the respiratory dysfunction, the increased glycolytic ATP, in the activated ECs, might compensate for the loss of mitochondrial produced ATP, leading to overall increased ATP production. Interestingly, ATP derived from mitochondrial OXPHOS in ECs was also shown to be involved in enhancing NO-dependent vasodilatory responses (Wilson et al., 2023). CPP-induced loss of OXPHOS would therefore not only imply further skewing towards glycolysis, but also have direct effects on endothelial function by reducing NO-dependent vasodilatation.

Another adverse effect of mPTP opening is a steep increase in ROS production (Brookes et al., 2004). ROS are detrimental to mtDNA as they can cause mutations and induce selective autophagy of mitochondria (mitophagy)

(Ashrafi & Schwarz, 2013; Qu et al., 2022). In line with this we observed a relative decrease in mtDNA content, reflecting reduced numbers of mitochondria after CPP exposure. Furthermore, ROS provoke oxidation of lipids in the mitochondrial membrane, such as cardiolipin, thereby promoting the release of cytochrome C (Brookes et al., 2004; Petrosillo et al., 2003). As cytochrome C release is pro-apoptotic, mPTP opening may result in ROS-induced cytochrome C release culminating in apoptosis induction (Brookes et al., 2004; Petrosillo et al., 2003). CPP exposure decreased EC viability which could be rescued with CSA, a mPTP inhibitor. This coincided with reduced endothelial activation marker ICAM-1 and chemokine CCL2 and CXCL8 expression, as well as reduced enrichment for inflammatory cell signalling pathways (e.g. TLR, NF-$\kappa$B). These data indicate that mPTP opening may play an important role in CPP-induced mitochondrial and endothelial dysfunction, thereby forming a putative target for intervention. Indeed, studies on mPTP targeting indicate that blocking mPTP opening is beneficial for mitochondrial function and cell survival. For example, it has been shown that by adding CSA or metformin to ECs exposed to high glucose levels, mPTP opening was prevented as well as cytochrome C decompartmentalization and cell death (Detaille et al., 2005). Likewise, when adding Imeglimin, a new class of glucose-lowering agents, to microvascular ECs exposed to high glucose levels (HMEC-1), ROS production decreased, and the mitochondrial permeability transition was inhibited due to mPTP blocking (Detaille et al., 2016). Additionally, in a small clinical trial it was shown that injection of cyclosporin, before undergoing percutaneous coronary intervention, was associated with a smaller cardiac infarct size compared to placebo, also supporting a relationship between mPTP opening and cardiovascular diseases (Piot et al., 2008). Whether blocking of the mPTP *in vivo* will be beneficial to impede CPP-induced mitochondrial dysfunction in ECs, and subsequent EC activation and dysfunction, remains to be elucidated.

It is still unclear how CPP-induced EC mitochondrial dysfunction might affect vascular remodelling, including VC, in CKD. It could be hypothesized that CPP-induced EC activation and to some extent EC loss due to apoptosis (both driven by mitochondrial dysfunction) might result in loss of barrier function. Due to impaired barrier function (Jiang et al., 2022), CPPs could more easily reach the vascular smooth muscle cells (VSMCs) and could possibly promote VC. Alternatively, EC dysfunction might lead to the release of pro-inflammatory/pro-calcifying factors from ECs, which in turn might affect VSMCs in a paracrine manner, thereby promoting VC development. In line with this, several studies have demonstrated EC-derived extracellular vesicles are able to promote VSMC calcification *in vitro* (Li et al., 2019; Lin et al., 2022; Qin et al., 2022). Whether similar mechanisms are involved in CPP-induced EC activation remains to be established. In addition, the protein ontology analysis of differentially expressed proteins reported here suggests adverse endothelial remodelling or transdifferentiation as proteins involved in connective tissue development and extracellular matrix production have increased abundance in CPP-stimulated ECs. Interestingly, these findings overlap with our previous observation that the vessel wall transcriptome adopts a vascular remodelling signature *in vivo* in vascular tissue of CKD patients (Feenstra et al., 2024) which warrants further investigation.

Two other investigations have used proteome approaches to investigate endothelial responses to CPPs at either the cell or cell organelle level (Shishkova et al., 2022, 2023), albeit in different EC types. Notably, when comparing the cellular proteomes reported here and in the literature (Shishkova et al., 2022), pathway enrichment for calcium signalling, mitochondrial respiration and EC activation commonly denominated the proteomes altered by CPP treatment. Moreover, in a mitochondrial-specific proteome analysis (Shishkova et al., 2023), increased pathway enrichment of mitochondrial $Ca^{2+}$ transport and uptake was found in CPP-stimulated ECs, whereas pathway enrichment for respiratory electron transport was decreased. These data further substantiate our findings that CPPs may contribute to mitochondrial $Ca^{2+}$ overload and disturbance of oxidative phosphorylation in ECs.

Although our data imply an important role for CPP-induced mitochondrial and EC dysfunction, some limitations need to be mentioned. A potential limitation may be the use of HUVECs for our investigations, which are veinous primary cells of fetal origin and may have limited relevance to arterial disease. Yet, ECs in culture have a highly similar proteomic makeup with only limited specific signatures between organs and donors (Groten et al., 2024), suggesting that only moderate EC-type-dependent responses can be expected *in vitro*. Indeed, the similar outcomes in pathway enrichment analyses from our study and Shishkova et al. (2022) reflect this similarity of response. Another limitation may be the absence of information on the physiological local concentration of CPPs on the endothelial surface in CKD patients. Although it is generally accepted that CPP levels are elevated in CKD patients and the *in vitro* concentrations used here are commonly used in the field, the need for future studies investigating the true tissue exposure to CPPs is evident. Last, we could not functionally validate that inhibition of mPTP opening by CSA reduced mitochondrial $Ca^{2+}$ influx because of unexpected toxicity evoked by the interaction of the two compounds, leaving the question open if mPTP opening and mitochondrial dysfunction are upstream or downstream of the calcium influx. Nonetheless, we show here that CPPs induce mitochondrial

and EC dysfunction culminating in EC activation and death.

In conclusion, the current study shows that CPPs cause cytosolic and mitochondrial calcium influx in ECs, which coincides with mitochondrial dysfunction and EC activation and partial EC loss. EC activation and loss could be prevented by mitochondria-targeted therapy using CSA. Preventing CPP-induced EC activation, dysfunction and cell loss by targeting mitochondria might be an attractive strategy to attenuate EC-dependent vascular remodelling (including VC) in CKD as well as CVD in general.

## References


Alam, M. M., Lal, S., FitzGerald, K. E., & Zhang, L. (2016). A holistic view of cancer bioenergetics: Mitochondrial function and respiration play fundamental roles in the development and progression of diverse tumors. *Clinical and Translational Medicine*, **5**(1), 3.

Ashrafi, G., & Schwarz, T. L. (2013). The pathways of mitophagy for quality control and clearance of mitochondria. *Cell Death and Differentiation*, **20**(1), 31–42.

Bravo, R., Vicencio, J. M., Parra, V., Troncoso, R., Munoz, J. P., Bui, M., Quiroga, C., Rodriguez, A. E., Verdejo, H. E., Ferreira, J., Iglewski, M., Chiong, M., Simmen, T., Zorzano, A., Hill, J. A., Rothermel, B. A., Szabadkai, G., & Lavandero, S. (2011). Increased ER–mitochondrial coupling promotes mitochondrial respiration and bioenergetics during early phases of ER stress. *Journal of Cell Science*, **124**(13), 2143–2152.

Brookes, P. S., Yoon, Y., Robotham, J. L., Anders, M. W., & Sheu, S.-S. (2004). Calcium, ATP, and ROS: A mitochondrial love-hate triangle. *American Journal of Physiology – Cell Physiology*, **287**(4), C817–C833.

Bundy, J. D., Cai, X., Scialla, J. J., Dobre, M. A., Chen, J., Hsu, C. Y., Leonard, M. B., Go, A. S., Rao, P. S., Lash, J. P., Townsend, R. R., Feldman, H. I., de Boer, I. H., Block, G. A., Wolf, M., Smith, E. R., Pasch, A., Isakova, T., & CRIC Study Investigators. (2019). Serum calcification propensity and coronary artery calcification among patients with CKD: The CRIC (Chronic Renal Insufficiency Cohort) Study. *American Journal of Kidney Diseases*, **73**(6), 806–814.

Bundy, J. D., Cai, X., Mehta, R. C., Scialla, J. J., de Boer, I. H., Hsu, C., Go, A. S., Dobre, M. A., Chen, J., Rao, P. S., Leonard, M. B., Lash, J. P., Block, G. A., Townsend, R. R., Feldman, H. I., Smith, E. R., Pasch, A., & Isakova, T. (2019). Serum calcification propensity and clinical events in CKD. *Clinical Journal of the American Society of Nephrology*, **14**(11), 1562–1571.

Burgess, W. H., Mehlman, T., Friesel, R., Johnson, W. V., & Maciag, T. (1985). Multiple forms of endothelial cell growth factor. Rapid isolation and biological and chemical characterization. *Journal of Biological Chemistry*, **260**(21), 11389–11392.

Deniaud, A., Sharaf el dein, O., Maillier, E., Poncet, D., Kroemer, G., Lemaire, C., & Brenner, C. (2008). Endoplasmic reticulum stress induces calcium-dependent permeability transition, mitochondrial outer membrane permeabilization and apoptosis. *Oncogene*, **27**(3), 285–299.

Detaille, D., Guigas, B., Chauvin, C., Batandier, C., Fontaine, E., Wiernsperger, N., & Leverve, X. (2005). Metformin prevents high-glucose–induced endothelial cell death through a mitochondrial permeability transition-dependent process. *Diabetes*, **54**(7), 2179–2187.

Detaille, D., Vial, G., Borel, A.-L., Cottet-Rouselle, C., Hallakou-Bozec, S., Bolze, S., Fouqueray, P., & Fontaine, E. (2016). Imeglimin prevents human endothelial cell death by inhibiting mitochondrial permeability transition without inhibiting mitochondrial respiration. *Cell Death Discovery*, **2**(1), 15072.

Elustondo, P. A., Nichols, M., Negoda, A., Thirumaran, A., Zakharian, E., Robertson, G. S., & Pavlov, E. V. (2016). Mitochondrial permeability transition pore induction is linked to formation of the complex of ATPase C-subunit, polyhydroxybutyrate and inorganic polyphosphate. *Cell Death Discovery*, **2**(1), 16070.

Feenstra, L., Reijrink, M., Pasch, A., Smith, E. R., Visser, L. M., Bulthuis, M., Lodewijk, M. E., Mastik, M. F., Greuter, M. J. W., Slart, R. H. J. A., Mulder, D. J., Pol, R. A., Te Velde-Keyzer, C. A., Krenning, G., Hillebrands, J. L., & TransplantLines Investigators. (2024). Calciprotein particle counts associate with vascular remodelling in chronic kidney disease. *Cardiovascular Research*, **120**(15), 1953–1966.

Feenstra, L., Kutikhin, A. G., Shishkova, D. K., Buikema, H., Zeper, L. W., Bourgonje, A. R., Krenning, G., & Hillebrands, J.-L. (2023). Calciprotein particles induce endothelial dysfunction by impairing endothelial nitric oxide metabolism. *Arteriosclerosis, Thrombosis, and Vascular Biology*, **43**(3), 443–455.

Feno, S., Butera, G., Vecellio Reane, D., Rizzuto, R., & Raffaello, A. (2019). Crosstalk between calcium and ROS in pathophysiological conditions. *Oxidative Medicine and Cellular Longevity*, **2019**, 1–18.

Fischer, R., & Kessler, B. M. (2015). Gel-aided sample preparation (GASP)-A simplified method for gel-assisted proteomic sample generation from protein extracts and intact cells. *Proteomics*, **15**(7), 1224–1229.

Giorgi, C., Marchi, S., & Pinton, P. (2018). The machineries, regulation and cellular functions of mitochondrial calcium. *Nature Reviews Molecular Cell Biology*, **19**(11), 713–730.

Groten, S. A., Smit, E. R., van den Biggelaar, M., & Hoogendijk, A. J. (2024). The proteomic landscape of in vitro cultured endothelial cells across vascular beds. *Communications Biology*, **7**(1), 989.

Holt, S. G., & Smith, E. R. (2016). Fetuin-A-containing calciprotein particles in mineral trafficking and vascular disease. *Nephrology Dialysis Transplantation*, **31**(10), 1583–1587.

Jiang, H., Li, L., Zhang, L., Zang, G., Sun, Z., & Wang, Z. (2022). Role of endothelial cells in vascular calcification. *Frontiers in Cardiovascular Medicine*, **9**, 1–17.

Keyzer, C. A., de Borst, M. H., van den Berg, E., Jahnen-Dechent, W., Arampatzis, S., Farese, S., Bergmann, I. P., Floege, J., Navis, G., Bakker, S. J. L., van Goor, H., Eisenberger, U., & Pasch, A. (2016). Calcification propensity and survival among renal transplant recipients. *Journal of the American Society of Nephrology*, **27**(1), 239–248.

Kolberg, L., Raudvere, U., Kuzmin, I., Adler, P., Vilo, J., & Peterson, H. (2023). G:profiler-interoperable web service for functional enrichment analysis and gene identifier mapping (2023 update). *Nucleic Acids Research*, **51**(W1), W207–W212.

Kutikhin, A. G., Velikanova, E. A., Mukhamadiyarov, R. A., Glushkova, T. V., Borisov, V. V., Matveeva, V. G., Antonova, L. V., Filip'ev, D. E., Golovkin, A. S., Shishkova, D. K., Burago, A. Y., Frolov, A. V., Dolgov, V. Y., Efimova, O. S., Popova, A. N., Malysheva, V. Y., Vladimirov, A. A., Sozinov, S. A., Ismagilov, Z. R., … Yuzhalin, A. E. (2016). Apoptosis-mediated endothelial toxicity but not direct calcification or functional changes in anti-calcification proteins defines pathogenic effects of calcium phosphate bions. *Scientific Reports*, **6**(1), 27255.

Kutikhin, A. G., Feenstra, L., Kostyunin, A. E., Yuzhalin, A. E., Hillebrands, J.-L., & Krenning, G. (2021). Calciprotein particles. *Arteriosclerosis, Thrombosis, and Vascular Biology*, **41**(5), 1607–1624.

Li, L., Wang, M., Ma, Q., Ye, J., & Sun, G. (2022). Role of glycolysis in the development of atherosclerosis. *American Journal of Physiology – Cell Physiology*, **323**(2), C617–C629.

Li, S., Zhan, J.-K., Wang, Y.-J., Lin, X., Zhong, J.-Y., Wang, Y., Tan, P., He, J.-Y., Cui, X.-J., Chen, Y.-Y., Huang, W., & Liu, Y.-S. (2019). Exosomes from hyperglycemia-stimulated vascular endothelial cells contain versican that regulate calcification/senescence in vascular smooth muscle cells. *Cell & Bioscience*, **9**(1), 1–15.

Lin, X., Shan, S.-K., Xu, F., Zhong, J.-Y., Wu, F., Duan, J.-Y., Guo, B., Li, F.-X.-Z., Wang, Y., Zheng, M.-H., Xu, Q.-S., Lei, L.-M., Ou-Yang, W.-L., Wu, Y.-Y., Tang, K.-X., Ullah, M. H. E., Liao, X.-B., & Yuan, L.-Q. (2022). The crosstalk between endothelial cells and vascular smooth muscle cells aggravates high phosphorus-induced arterial calcification. *Cell Death & Disease*, **13**(7), 650.

Marreiros, C., Viegas, C., & Simes, D. (2022). Targeting a silent disease: Vascular calcification in chronic kidney disease. *International Journal of Molecular Sciences*, **23**(24), 16114.

Matuz-Mares, D., González-Andrade, M., Araiza-Villanueva, M. G., Vilchis-Landeros, M. M., & Vázquez-Meza, H. (2022). Mitochondrial calcium: Effects of its imbalance in disease. *Antioxidants*, **11**(5), 801.

Medina-Leyte, D. J., Zepeda-García, O., Domínguez-Pérez, M., González-Garrido, A., Villarreal-Molina, T., & Jacobo-Albavera, L. (2021). Endothelial dysfunction, inflammation and coronary artery disease: Potential biomarkers and promising therapeutical approaches. *International Journal of Molecular Sciences*, **22**(8), 3850.

Mootha, V. K., Lindgren, C. M., Eriksson, K. F., Subramanian, A., Sihag, S., Lehar, J., Puigserver, P., Carlsson, E., Ridderstråle, M., Laurila, E., Houstis, N., Daly, M. J., Patterson, N., Mesirov, J. P., Golub, T. R., Tamayo, P., Spiegelman, B., Lander, E. S., Hirschhorn, J. N., Altshuler, D., & Groop, L. C. (2003). PGC-1$\alpha$-responsive genes involved in oxidative phosphorylation are coordinately downregulated in human diabetes. *Nature Genetics*, **34**(3), 267–273.

Murphy, E., & Liu, J. C. (2023). Mitochondrial calcium and reactive oxygen species in cardiovascular disease. *Cardiovascular Research*, **119**(5), 1105–1116.

Nakamura, K., Isoyama, N., Nakayama, Y., Hiroyoshi, T., Fujikawa, K., Miura, Y., Kurosu, H., Matsuyama, H., & Kuro-o, M. (2022). Association between amorphous calcium-phosphate ratios in circulating calciprotein particles and prognostic biomarkers in hemodialysis patients. *Scientific Reports*, **12**(1), 13030.

Panda, S., Behera, S., Alam, M. F., & Syed, G. H. (2021). Endoplasmic reticulum & mitochondrial calcium homeostasis: The interplay with viruses. *Mitochondrion*, **58**, 227–242.

Petrosillo, G., Ruggiero, F. M., & Paradies, G. (2003). Role of reactive oxygen species and cardiolipin in the release of cytochrome c from mitochondria. *The Federation of American Societies for Experimental Biology Journal*, **17**(15), 2202–2208.

Piot, C., Croisille, P., Staat, P., Thibault, H., Rioufol, G., Mewton, N., Elbelghiti, R., Cung, T. T., Bonnefoy, E., Angoulvant, D., Macia, C., Raczka, F., Sportouch, C., Gahide, G., Finet, G., André-Fouët, X., Revel, D., Kirkorian, G., Monassier, J. P., … Ovize, M. (2008). Effect of cyclosporine on reperfusion injury in acute myocardial infarction. *New England Journal of Medicine*, **359**(5), 473–481.

Qin, Z., Li, Y., Li, J., Jiang, L., Zhang, Z., Chang, K., Yang, Q., Chen, S., Liao, R., & Su, B. (2022). Exosomal STAT1 derived from high phosphorusstimulated vascular endothelial cells induces vascular smooth muscle cell calcification via the wnt/$\beta$catenin signaling pathway. *International Journal of Molecular Medicine*, **50**(6), 139.

Qu, K., Yan, F., Qin, X., Zhang, K., He, W., Dong, M., & Wu, G. (2022). Mitochondrial dysfunction in vascular endothelial cells and its role in atherosclerosis. *Frontiers in Physiology*, **13**, 1–20.

Rossi, A., Pizzo, P., & Filadi, R. (2019). Calcium, mitochondria and cell metabolism: A functional triangle in bioenergetics. *Biochimica et Biophysica Acta (BBA) – Molecular Cell Research*, **1866**(7), 1068–1078.

Santulli, G., Xie, W., Reiken, S. R., & Marks, A. R. (2015). Mitochondrial calcium overload is a key determinant in heart failure. *Proceedings of the National Academy of Sciences*, **112**(36), 11389–11394.

Schneider, C. A., Rasband, W. S., & Eliceiri, K. W. (2012). NIH image to ImageJ: 25 years of image analysis. *Nature Methods*, **9**(7), 671–675.

Schnitzler, J. G., Hoogeveen, R. M., Ali, L., Prange, K. H. M., Waissi, F., van Weeghel, M., Bachmann, J. C., Versloot, M., Borrelli, M. J., Yeang, C., de Kleijn, D. P. V., Houtkooper, R. H., Koschinsky, M. L., de Winther, M. P. J., Groen, A. K., Witztum, J. L., Tsimikas, S., Stroes, E. S. G., & Kroon, J. (2020). Atherogenic lipoprotein(a) increases vascular glycolysis, thereby facilitating inflammation and leukocyte extravasation. *Circulation Research*, **126**(10), 1346–1359.

Shishkova, D., Lobov, A., Repkin, E., Markova, V., Markova, Y., Sinitskaya, A., Sinitsky, M., Kondratiev, E., Torgunakova, E., & Kutikhin, A. (2023). Calciprotein particles induce cellular compartment-specific proteome alterations in human arterial endothelial cells. *Journal of Cardiovascular Development and Disease*, **11**, 5.

Shishkova, D., Lobov, A., Zainullina, B., Matveeva, V., Markova, V., Sinitskaya, A., Velikanova, E., Sinitsky, M., Kanonykina, A., Dyleva, Y., & Kutikhin, A. (2022). Calciprotein particles cause physiologically significant pro-inflammatory response in endothelial cells and systemic circulation. *International Journal of Molecular Sciences*, **23**(23), 14941.

Shishkova, D. K., Velikanova, E. A., Bogdanov, L. A., Sinitsky, M. Y., Kostyunin, A. E., Tsepokina, A. V., Gruzdeva, O. V., Mironov, A. V., Mukhamadiyarov, R. A., Glushkova, T. V., Krivkina, E. O., Matveeva, V. G., Hryachkova, O. N., Markova, V. E., Dyleva, Y. A., Belik, E. V., Frolov, A. V., Shabaev, A. R., Efimova, O. S., … Kutikhin, A. G. (2021) Calciprotein particles link disturbed mineral homeostasis with cardiovascular disease by causing endothelial dysfunction and vascular inflammation. *International Journal of Molecular Sciences*, **22**(22), 12458.

Smith, E. R., Ford, M. L., Tomlinson, L. A., Bodenham, E., McMahon, L. P., Farese, S., Rajkumar, C., Holt, S. G., & Pasch, A. (2014). Serum calcification propensity predicts all-cause mortality in predialysis CKD. *Journal of the American Society of Nephrology*, **25**(2), 339–348.

Smith, E. R., Ford, M. L., Tomlinson, L. A., Rajkumar, C., McMahon, L. P., & Holt, S. G. (2012). Phosphorylated fetuin-A-containing calciprotein particles are associated with aortic stiffness and a procalcific milieu in patients with pre-dialysis CKD. *Nephrology Dialysis Transplantation*, **27**(5), 1957–1966.

Subramanian, A., Tamayo, P., Mootha, V. K., Mukherjee, S., Ebert, B. L., Gillette, M. A., Paulovich, A., Pomeroy, S. L., Golub, T. R., Lander, E. S., & Mesirov, J. P. (2005). Gene set enrichment analysis: A knowledge-based approach for interpreting genome-wide expression profiles. *Proceedings of the National Academy of Sciences*, **102**(43), 15545–15550.

Sun, H.-J., Wu, Z.-Y., Nie, X.-W., & Bian, J.-S. (2020). Role of endothelial dysfunction in cardiovascular diseases: The link between inflammation and hydrogen sulfide. *Frontiers in Pharmacology*, **10**, 1–15.

Thiem, U., Hewitson, T. D., Toussaint, N. D., Holt, S. G., Haller, M. C., Pasch, A., Cejka, D., & Smith, E. R. (2023). Effect of the phosphate binder sucroferric oxyhydroxide in dialysis patients on endogenous calciprotein particles, inflammation, and vascular cells. *Nephrology Dialysis Transplantation*, **38**(5), 1282–1296.

Tran, Q. K., Ohashi, K., & Watanabe, H. (2000). Calcium signalling in endothelial cells. *Cardiovascular Research*, **48**(1), 13–22.

Wilson, C., Lee, M. D., Buckley, C., Zhang, X., & McCarron, J. G. (2023). Mitochondrial ATP production is required for endothelial cell control of vascular tone. *Function*, **4**(2), zqac063.

Xiao, W., Oldham, W. M., Priolo, C., Pandey, A. K., & Loscalzo, J. (2021). Immunometabolic endothelial phenotypes: Integrating inflammation and glucose metabolism. *Circulation Research*, **129**(1), 9–29.

Zhou, Y., Jing, S., Liu, S., Shen, X., Cai, L., Zhu, C., Zhao, Y., & Pang, M. (2022). Double-activation of mitochondrial permeability transition pore opening via calcium overload and reactive oxygen species for cancer therapy. *Journal of Nanobiotechnology*, **20**(1), 188.

## Additional information

### Data availability statement

The raw MS data are available at https://www.iprox.cn/page/home.html (IPX0007030001). Other data related to this paper are available upon reasonable request to the corresponding author.

### Competing interests

G. Krenning is the Chief Scientific Officer of Sulfateq B.V. (Groningen, the Netherlands), a company that develops small-molecule therapeutics. Sulfateq B.V. has no small molecule in development for anti-circulating calciprotein particle (CPP) therapy at present and had no influence on the content of this article. The other authors report no conflict of interest.

### Author contributions

L.F., experiments, data acquisition, data analysis, manuscript preparation and writing; L.C., B.B. and J.P., proteome analysis, data acquisition and primary analysis; M.F.M. and A.v.B., technical support with NanoString analysis and Oroboros O2k experiments; D.N. and B.S.S., experiments, primary data analysis; J.L.H. conception, experimental design, writing, revising, supervision; G.K., corresponding author, conception, experimental design, data analysis, supervision, writing and revising. All authors approved the final version of the manuscript.

### Funding

Financial support for this study was provided to L. Feenstra by the Graduate School of Medical Sciences of the University of Groningen, the Netherlands. Proteome analysis was supported by a grant from the De Cock – Hadders Scientific

Research Foundation, the Netherlands. L. Chatre was financially supported by the CNRS. B. S. Star was financially supported by an MD/PhD grant from the UMCG. Dalibor Nakládal was financially supported by the European Union's Horizon 2020 research and innovation programme on the basis of a grant agreement under the Marie Skłodowska-Curie funding scheme No. 945478; by the Slovak Academic and Scientific Programme No. 3333/03/02; and by the Slovak Research and Development Agency No. PP-MSCA-2022-0001. J. L. Hillebrands is the principal investigator in the NIGRAM2+ (NIer Gerichte Research van Arterie tot Mens: centrale rol voor Magnesium ++) consortium, funded by Health Holland (LSHM17034) and the Dutch Kidney Foundation (16TKI02). Part of the work was performed in the UMIC, sponsored by NWO 175-010-2009-023.

## Acknowledgements

We would like to thank Klaas Sjollema UMCG Microscopy and Imaging Center (UMIC Center, UMCG, the Netherlands) for technical support during image acquisition. We thank Monique Lodewijk, Josée Plantinga, Rianne Jongman and Timara Kuiper for technical support in the lab, and Jade Talavera for his help with data analysis regarding mitochondrial network quantification (all UMCG, the Netherlands). The *Ru265* compound was kindly provided by Prof. A. M. Dolga from the Department of Molecular Pharmacology (UMCG, the Netherlands).

## Keywords

calciprotein particle (CPP), calcium ion, chronic kidney disease (CKD), endothelial cell, mitochondrial dysfunction, mitochondrion, vascular calcification

## Supporting information

Additional supporting information can be found online in the Supporting Information section at the end of the HTML view of the article. Supporting information files available:

**Peer Review History**
**Supplementary Information**